

Cortical Lead Fields of Electroencephalographic and Magnetoencephalographic Sensors

Andrei Irimia^{1*}, Zeynep Akalin Acar^{2,3}, Donald J. Hagler Jr.¹,
Anders M. Dale^{1,4,5}, Ming Xiong Huang⁶, Eric Halgren^{1,4}

¹Multimodal Imaging Laboratory, Department of Radiology, University of California, San Diego, La Jolla, California, 92093, USA

²Swartz Center for Computational Neuroscience, University of California, San Diego, La Jolla, California, 92093, USA

³Institute for Neural Computation, University of California, San Diego, La Jolla, California, 92093, USA

⁴Department of Neurosciences, University of California, San Diego, La Jolla, California, 92093, USA

⁵Department of Cognitive Science, University of California, San Diego, La Jolla, California, 92093, USA

⁶Radiology Imaging Laboratory, Department of Radiology, University of California, San Diego, La Jolla, California, 92093, USA

Running title: Cortical lead fields of EEG and MEG sensors

*To whom correspondence should be addressed.

Andrei Irimia, Ph.D.

Laboratory of Neuro Imaging

Department of Neurology

University of California, Los Angeles

635 Charles E. Young Drive South

Suite 225

Los Angeles CA 90095

andrei.irimia@loni.ucla.edu

Phone: (01) (310) 206-2101

Fax: (01) (310) 206-5518

Abstract

The spatial relationship of electroencephalography (EEG) and magnetoencephalography (MEG) to brain activation is quantified as their cortical lead fields: the sensitivity of each sensor to activation of each cortical location. Here we map the lead fields of EEG and MEG across the cortical surface using a realistic boundary element model with four compartments. These calculations demonstrate that inclusion of CSF is essential for accurate calculation of EEG lead fields. The typical referential EEG derivation is affected by activity in all lobes of both hemispheres, while the typical MEG planar gradiometer is sensitive to part of one lobe. The proportion of cortical dipoles that have an effect on the average sensor that is $\geq 25\%$ of the most effective dipole, is $\sim 40\%$ for referential EEG and $< 2\%$ for MEG gradiometers. Gradiometers are substantially more focal than magnetometers and both are typically more focal than EEG. These findings indicate that gradiometer signals usually arise from the underlying cortex and that their coherence can often be inferred to reflect neural interaction rather than overlapping lead fields; such inferences are unwarranted for referential EEG. Quantitative differences between EEG and MEG lead fields may give rise to qualitative differences in the neural systems that they record.

Keywords

EEG, MEG, modeling, neuroimaging, synchrony

Electroencephalography (EEG) and magnetoencephalography (MEG) are complementary neuroimaging techniques that are widely used to investigate brain activity at a millisecond resolution which is unavailable to functional magnetic resonance imaging (fMRI) (Dale 2001). Conversely, the spatial resolutions of MEG and EEG are indeterminate, and their imputed generators are dependent on the assumptions used for their localization. There is, however, a minimum level of certainty that is set by biological constraints on possible generators of EEG and MEG, and by biophysical constraints on the spatial sensitivity of each sensor.

The generators of neuronal currents within the frequency range of EEG and MEG are trans-membrane post-synaptic currents due to post-synaptic ligand-gated and active voltage-gated channels (Murakami 2003; Murakami 2002). These active trans-membrane currents lead to intracellular currents and passive returns across the membrane with a distribution that depends on the shape of the neuron (Einevoll 2007). The intracellular limb of this current is thought to generate the MEG and the extracellular limb the EEG (Hamalainen, et al. 1993). However, these currents will only summate to produce measurable signals if they are spatially aligned, and this is in most cases restricted in the brain to the apical dendrites of neocortical pyramidal cells. In addition, the EEG and MEG signals decline by the square of the distance from the generator, and nearly all of the gray matter that is close to the EEG or MEG sensors is cortical. Thus, it is reasonable in most analyses to constrain possible generators of MEG and EEG to dipoles that are in the cortex and perpendicular to its local surface (Dale and Sereno 1993).

The task of localizing electric currents based on the measurement of the electric potentials (EEG) or magnetic fields (MEG) that they generate is known as the inverse problem of bioelectromagnetism. This problem is ill-posed, which means that an infinity of solutions exist unless specific assumptions are made regarding the nature of the sources—for example, their number and correlations for methods that assume few dipoles, and the quantity being minimized (power or current) for methods that estimate activation at all locations. In addition, the inverse solution is dependent on a forward model which specifies the manner in which EEG/MEG measurements are assumed to arise from underlying currents, based on the anatomy of the head, the conductance of its constituent tissues, and the equations used to calculate the passage of current through these spaces. A realistic forward model is critical for inverse solution accuracy.

One advantage of MEG over EEG is that, while electric potentials are much attenuated by the presence of multiple conductive layers interposed between cortex and electrodes, magnetic fields are primarily dependent on tissue permeability, which in the case of biological matter is almost equal to that of free space (μ_0). Conversely, the attenuating and smearing effects of head layers upon EEG measurements result in a large sensitivity of EEG inverse estimates to the anatomical accuracy of the forward model (Laarne 1999). A number of studies ((Ramon 2006a; Ramon 2006b; Wendel 2008) and references therein) have proposed that the omission of head layers from the forward model or the inadequate modeling of their physical properties (especially their conductivity) can result in large systematic errors in source localization. The importance of forward model accuracy has gained greater appreciation in recent years, particularly with the publication of studies (Ramon 2007; Ramon 2004) which underline the consequences of omitting the effect of the cerebrospinal fluid (CSF) in the forward EEG model. The CSF layer (though thin compared to the skull) exhibits relatively high conductivity (~ 1.79 S/m) compared to skin (~ 0.3 S/m) or bone (Baumann 1997; Wendel 2008), which causes significant diffusion of the electric current. Thus, excluding the CSF layer leads to underestimation of electric conduction effects, with consequent effects on EEG inverse solutions.

The importance of CSF in EEG modeling has often been understated, partly due to the challenge of segmenting the CSF layer from T1- and T2-weighted MR images, partly due to the high mesh refinement required to model the CSF layer, and partly due to the assumption that its thinness prevents it from playing a significant role in conduction. However, recent studies found that source strengths could be underestimated by as much as 300-500% when inverse models without the CSF layer were used (Ramon 2007; Ramon 2004; Rullmann 2009; Wendel 2008). Consequently, several previous assessments of EEG—particularly concerning its relative focality compared to MEG—may need to be revisited. In this article, we map for the first time, the cortical area whose neuronal sources contribute to the signal recorded by each given EEG or MEG sensor (i.e. the ‘cortical lead field’ of the device) using an anatomically realistic Boundary Element Model (BEM) that includes the conductive effect of the CSF layer and individually-reconstructed cortical surfaces. Novel metrics (‘focality,’ ‘sensor sensitivity area,’ ‘orientation cancellation index,’ and ‘global sensitivity’) are introduced to facilitate comparison of these maps. We find that the cortical lead fields of MEG gradiometers are smaller than the corresponding areas for EEG referential derivations. Specifically, the lead fields of MEG gradiometers are focal in the cortex directly underlying the sensor, in contrast to the lead fields of EEG referential derivations which include large regions of multiple lobes in both hemispheres. We also investigate the MEG

magnetometers, and bipolar as well as Laplacian EEG derivations. While these give intermediate values between gradiometers and referential derivations, in nearly all comparisons, MEG measures are more focal than EEG. The cortical lead field maps provided here should provide useful insights for interpreting EEG and MEG signals.

Materials and Methods

Analytic EEG modeling

To investigate the effect of CSF upon EEG, the analytic models of Zhang (Zhang 1995) and Berg & Scherg (Berg 1994) were used to calculate the EEG potentials due to current dipoles located within multilayer isotropic spheres. These models are based on extensions of the formulas for a dipole within a homogeneous sphere (de Munck 1991). The conductivity ratios 1:6:0.0133:1 (Baumann 1997; Geddes 1967) were assumed for brain:CSF, CSF:skull, and skull:scalp spheres, respectively, and simulations conducted using skull:brain conductivity ratios ranging from 20 to 80 yielded similar results, both qualitatively and quantitatively. All shells were concentric and their conductivities were assumed to be homogeneous. The values chosen for the radii of the brain, CSF, skull and scalp spheres were 7, 7.1, 7.8 and 8.5 cm, respectively, and 24,000 dipoles were positioned uniformly at a depth of 2 mm below the surface of the brain sphere (1.7 cm below the surface of the outermost layer). Dipoles were directed outwards and their orientations were normal with respect to each spherical surface. EEG sensors were assumed to be positioned on the outermost (scalp) shell. For comparison, a similar model was created without CSF. In the latter case, the conductivity of the CSF shell was assumed to be identical to that of the brain shell.

Realistic modeling

The electromagnetic field of the brain was recorded with 306 MEG and 60 EEG channels from 7 healthy adults (4 males, 3 females, ages 20-35) with a whole-head Elekta Neuromag® scanner within a magnetically shielded room (IMEDCO, Högendorf, Switzerland). SQUID (Superconducting QUantum Interference Device) sensors were arranged as triplets at 102 locations; each location contained one magnetometer (MAG) and two orthogonal planar gradiometers (GRAD1, GRAD2). The lead fields in the plane of each type of sensor are shown in Figure 1.

Figure 1 goes about here.

EEG sensors were placed according to the 10-20 system (Jasper 1974). 'Referential' (monopolar) EEG recordings were referenced to averaged mastoid, while 'bipolar' recordings were differential between the adjacent scalp locations using the standard 'super-banana' montage. For 'Laplacian' EEG, the nearest-neighbor method (Hjorth 1975; Wallin 1980) was used because it is simplest and most common (Lagerlund 1999); in this approach, the EEG signal is computed as the center electrode potential minus the average potential at the four neighbors. Electrode locations on the scalp of individual subjects were recorded using a 3D digitizer (Polhemus FastTrack®, Colchester, VT), while head position index (HPI) coils were used to measure the spatial relationship between the head and MEG scanner. T1 MR volumes were acquired at 1.5 T using the MP RAGE sequence or equivalent (Mugler 1990). Images were segmented in FreeSurfer (Dale, et al. 1999) and the tessellated border between white and gray matter was chosen as the representative cortical surface for the purpose of forward modeling (Dale and Sereno 1993).

Examples of BEM meshes created with our processing stream are shown in Figure 2. The tessellated surface of white-gray matter border in each hemisphere had ~150,000 vertices and provided a spacing of ~1 mm between seeded dipoles across the cortical surface (accurate enough to capture the anatomy of cortical regions with large curvature, such as the crowns of gyri or the bottoms of sulci; see Figure 2). Whereas the brain was segmented in FreeSurfer, the other meshes were segmented using the algorithm of Akalin Acar & Gençer (Akalin-Acar 2004) and the Neuroelectromagnetic Forward modeling Toolbox (NFT) of Akalin Acar & Makeig ((Akalin-Acar 2008; Akalin-Acar 2010), freely available at <http://sccn.ucsd.edu/nft/>). The scalp, inner and outer skull shells each had ~15,000 vertices (range: 13,200 to 17,700 vertices) to prevent numerical instabilities from occurring at the boundary between layers, where conductivity changes are large (Fuchs 2001; Laarne 1999; Yvert 1995; Yvert 2001). In the case of the CSF layer (range: ~6800 to ~7300 vertices), the adaptive recursive integration technique of Frijns et al. (Frijns 2000) was used to divide surface elements into sub-elements and to perform numerical integration recursively until convergence.

Figure 2 goes about here.

To register EEG sensors to each individual's cortical surface, a common procedure described in (Hamalainen, et al. 1993) was followed. Nasion, right and left PA coordinates were recorded with the digitizer and then identified on the subject's T1 MR image to generate a rigid registration matrix between EEG and MRI coordinate systems. Additional digitized points (the 60 EEG electrodes, 4 HPI coils, and other points on the subject's scalp) add to the accuracy of the registration. In the case of MEG, the head was assumed to be positioned optimally under the scanner to simulate the ideal scenario in which the distance from the recording point to the scalp is roughly the same for as many sensors as possible (see Figure 2). Across sensors and subjects, the minimum distance from each sensor to the scalp was 2.89 ± 0.79 cm (mean and standard deviation), while the corresponding values for the distance from each sensor to the brain was 4.92 ± 1.12 cm. Making this assumption does not entail altering the relative location of sensors with respect to other sensors; in other words, it does not require a spatial arrangement of the sensors that is different from the true one. The constraint of ideal head location is necessary in order to avoid bias due to preferential focality of MEG to parts of the head that are closest to the scanner. We also explicitly analyze the effect of moving the MEG sensors away from the head.

Because realistically shaped models have higher prediction accuracy for source localization compared to spherical shell models (Buchner 1995; Meijs, et al. 1987; Mosher 1999a; Mosher 1999b; Mosher, et al. 1999; Stok, et al. 1986), a four-shell, realistically shaped boundary element model (BEM) was used for the head. The BEM was constructed from tessellated surfaces of the inner-skull, CSF, outer-skull and outer-skin (scalp) generated from MRI (examples are shown in Figure 2). In the case of MEG, a one-shell BEM was used, as it is known to have adequate accuracy for forward calculations (Hamalainen, et al. 1993; Meijs, et al. 1987; Stok, et al. 1986). The conductivity ratios 1:0.1676:0.0125:1 (as in the analytic case above) were assumed for brain to CSF, CSF to skull, and skull to scalp, respectively. The BEM model was used to generate the forward matrix \mathbf{A} , an array of dimensions $M \times N$, where M is the number of sensors and N is the number of sources. For each source j , the column \mathbf{a}_j of the forward matrix specifies the projection of that source onto the sensors, i.e. the relationship between the source and the physical quantity measured at each sensor. Thus, the forward matrix provides the linear transformation from source space to sensor space. Forward calculations used the linear collocation method (Mosher 1999c) and the isolated skull approach (Meijs 1989), as they have been shown to provide reasonable accuracy (Yvert 1996; Yvert 2001). To accomplish cortical averaging over subjects, an average folding pattern (atlas) was first generated over a large number of individual subjects as a function on the unit sphere using the methods of Fischl, Dale et al. (Dale, et al. 1999; Fischl, et al. 1999a; Fischl, et al. 1999b), whereafter each individual was non-rigidly aligned with the atlas in a manner that aligned sulcal-gyral patterns while minimizing shear and areal distortion. Automatic parcellation of gyri and sulci was performed in FreeSurfer using probabilistic labeling on the statistical surface-based atlas of Fischl et al. (Fischl 2004).

Fuchs et al. (Fuchs 2001) made the pertinent observation that adequate refinement of the outer shells is important for forward model accuracy. They determined that large errors in the forward solution can occur if the inner skull mesh is too coarse and concluded that it is favorable to set up the outer compartments using meshes with at least 1,000 nodes. Here, we confirm this observation and note that our own forward EEG models can misestimate EEG potentials by as much as 10-15% if outer shells with fewer than 1,000 nodes are employed. It was found that this problem could be optimally addressed by using BEM's with ~7,000 nodes for the CSF and inner skull shells, and ~4,500 for the outer skull and scalp. In the former two cases, the quoted resolution was found to be necessary because the relative thinness of the corresponding compartments could lead to numerical instability in the forward calculation. In the case of MEG, on the other hand, it was found that the use of a single (inner skull) shell with about 2,500 nodes was appropriate and sufficient. Specifically, calculations using more refined meshes yielded changes in the estimated potentials and fields of less than 1%.

Cortical lead fields

To quantify the performance of EEG and MEG, one can define the 'cortical lead field' of a particular sensor as the strength and direction associated with the projection of each cortical source to that sensor ((Liu, et al. 1998; Malmivuo 1980; Rush 1969); see also (Lutkenhoener 1997) for the related concept of the resolution field). The lead field is directly calculated from the forward matrix \mathbf{A} (Hillebrand 2002). For any sensor i , let \mathbf{a}_i denote the i -th row of \mathbf{A} . Similarly, let \mathbf{a}_j denote the j -th column of \mathbf{A} . The entries a_{ij} (where $i = 1, \dots, M$ and $j = 1, \dots, N$) can be thought of as specifying the *cortical lead field vectors* (projections of each cortical dipole j onto

sensor i) and the absolute values of the vector \mathbf{a}_i (i.e. $|\mathbf{a}_i|$, the set of vectors for every point on the cortex) collectively represent the (scalar) *cortical lead field* for that sensor. One can thus relate the vector length of each dipole as “viewed” at the sensor as a color map, scaled to the magnitude of the largest dipole projection onto that sensor (Malmivuo 1997). Examples of scalar cortical lead field maps are shown in figure 3.

As explained in the introduction, measurable M/EEG signals are primarily due to electric currents produced by the spatially aligned apical dendrites of neocortical pyramidal cells. To reflect this, dipole orientation was assumed to be normal with respect to the cortical surface for this study. The direction of the dipole, toward or away from the local cortical surface, can be color coded, yielding oriented cortical lead field maps, examples of which are shown in figure 4.

To quantify how dipole orientation (into or out of the cortex) can affect cancellation of sources at the sensor, we introduce the *Orientation Cancellation Index (OCI)* (related to the Cancellation Index of Ahlfors et al. (Ahlfors 2009)) as

$$OCI(\mathbf{a}_i) = 1 - \left| \frac{\sum_{j=1}^N a_{ij}}{\sum_{j=1}^N |a_{ij}|} \right|, \quad (1)$$

For any sensor i , the numerator of the ratio above is the sum over the signed forward matrix elements associated with that sensor, whereas the denominator is the sum over the absolute values of these matrix elements. Each dipole is constrained to have normal orientation with respect to the cortical surface and, by convention, the matrix element a_{ij} is positive (or negative, respectively) if the normal component of dipole j which is detectable by sensor i is oriented out of (or into, respectively) the cortex. Consequently, if the detectable normal component points out of the cortex for all dipoles (or alternatively, if the component points into the cortex for all dipoles), then $OCI(i) = 0$. If there is an equal number of positive and negative matrix elements (outwardly and inwardly-oriented detectable normal components, respectively), then $OCI(i) = 1$. Thus the OCI quantifies the extent to which simultaneously active cortical sources have the ability to cancel each other out at the sensor. We map the topography of the OCI for different sensors in figure 6.

By combining the cortical lead fields of all sensors, one can create and visualize on the cortical surface a “total” lead field for each modality of choice. First, for each cortical source j , its average contribution to every sensor i was calculated as the *global sensitivity index (GSI)*, given by

$$GSI(\mathbf{a}_j) = \left[\left(\frac{1}{M} \sum_{i=1}^M |a_{ij}| \right)^2 \right]^{1/2}, \quad (2)$$

which is the root mean square (RMS) over all sensors $i = 1, \dots, M$ of the cortical lead fields $|\mathbf{a}_i|$. The GSI measure allows one to quantify how sensitive a certain modality is “on average” to the signal generated by each cortical dipole. Nevertheless, one disadvantage of this measure remains that it only provides insight about the measurement modality as a whole, whereas it does not allow one to distinguish between the (possibly contrasting) measurement abilities of different sensors. To investigate the capacity of each technique to record from various brain areas, the GSI was mapped across the entire cortex. In addition, the probability distribution function (PDF) of the GSI was computed for each measurement modality. The mean and standard deviation were also found for several cortical regions to illustrate the contrasting abilities of EEG and MEG to record from various anatomical structures of interest. These data are mapped and plotted in figures 6 and 7.

To quantify the focality of the cortical lead field of each sensor, we introduce and compute the *focality measure* F_i where, for some sensor i , F_i is the sum from 1 to N (the number of sources) of all values in the cortical lead field vector $|\mathbf{a}_i|$ normalized by the number of sources N and by the largest value in $|\mathbf{a}_i|$. That is,

$$F_i = \frac{1}{N \max\{|\mathbf{a}_i|\}} \sum_{j=1}^N |a_{ij}| \quad (3)$$

Since this can also be written as

$$F_i = \frac{1}{\max\{|\mathbf{a}_i|\}} \langle |\mathbf{a}_i| \rangle \quad (4)$$

it follows that F_i is simply the normalized average lead field magnitude. If the maximally sensitive sensor were responsive to only one dipole, its F would be equal to one divided by the number of dipoles ($\sim 300,000$ in our study), or approximately zero. At the other extreme, if all dipoles contributed equally to a sensor, then its F would be equal to 1. Thus, F varies from 0 to 1, with smaller numbers indicating more focal cortical lead fields.

To further explore the focality of different measurement modalities, we also introduce the *Sensor Sensitivity Area (SSA)* measure. SSA is an extension of the ‘half-sensitivity area’ introduced by Srinivasan et al. in (Srinivasan 2007), which is an extension of the ‘half-sensitivity volume’ used by Malmivuo and Plonsey (Malmivuo 1995) to characterize lead fields. The SSA is also similar to the ‘effective area’ measure of Cuffin & Cohen (Cuffin 1979). SSA curves are calculated from the lead field by determining the cortical dipoles that

project to a given sensor with a strength that is at least $x\%$ as strong as the dipole that projects most strongly to that sensor. This is averaged across all sensors for a given modality and expressed as percentage of total cortical area. Formally, the SSA is the cortical area that is populated with dipoles j whose projected signal strengths $|a_{ij}|$ at sensor i are greater than or equal to $x\%$ of the maximum projected signal of any dipole j on the cortex. This is equivalent to one minus the cumulative distribution function of the lead fields. In the limit as x approaches 100%, the SSA always approaches 0, because no dipole can project to the sensor more strongly than the strongest does; in the limit as x approaches 0%, the SSA always approaches 100%, because all dipoles do project at least that strongly. Between these trivial limits, the more focal measurement modalities will be characterized by smaller SSA values. When $x = 50\%$, the SSA equals the 'half-sensitivity area' (Srinivasan 2007). In order to facilitate the comparison of different models or modalities, the ratios of SSA curves for each value of x are also plotted. These data are shown in figures 8 and 9.

To explore the dependence of the SSA measure upon the distance d from MEG sensor to scalp, the SSA curves were also computed for increasing d ($d = 1, \dots, 5$ cm) using a simulated sensor located above the left hemisphere, approximately above the junction between the central sulcus and the Sylvian fissure. These data and the location of the simulated sensor relative to the head and brain are shown in Figure 10.

Results

Cortical lead fields

Examples of sensor lead fields are shown in Figure 3, where each row corresponds to a different modality (referential EEG, bipolar EEG, Laplacian EEG, magnetometer MEG and gradiometer MEG). Here and throughout, gradiometers are understood to be planar unless specified otherwise. The values plotted on the white matter surface in our figure are the absolute values of the forward matrix elements for a particular sensor i (i.e. $|\mathbf{a}_i|$, the set of lead field magnitudes associated with the sensor i of interest). Because the forward matrix elements specify how visible every source is at each sensor, plots of the cortical lead field are an indication of how many sources may contribute to the signal recorded at a given sensor. Examination of Figure 3 reveals that MEG lead fields are strikingly more focal than EEG lead fields. For example, the referential EEG cortical lead field shown in Figure 3 is for electrode C3 located above the precentral cortex of the left hemisphere; nevertheless, this electrode is sensitive to sources distributed over essentially the entire left hemisphere as well as to significant portions of the right hemisphere. The cortical lead fields for bipolar EEG are smaller than those for referential EEG, but still include large portions of both hemispheres. Lead fields for the Laplacian derivation are more focal than either referential or bipolar EEG, as was expected.

Figure 3 goes about here.

Figure 3 also illustrates how magnetometer cortical lead fields are not only larger than gradiometer lead fields, but have a significantly different shape as was expected given their contrasting sensitivities as shown in Figure 1. Magnetometers measure $\mathbf{B} \cdot \hat{\mathbf{n}} = B_z$, i.e. the component of the magnetic field that is (roughly) normal with respect to the surface of the head. On the other hand, the planar gradiometers of the Elekta Neuromag system measure either dB_z/dx or dB_z/dy , i.e. the derivatives of the normal component of the magnetic field along the coordinate axes that are tangential with respect to the surface of the head ((Nenonen 2004) contains a detailed description of this system). For magnetometers, Figure 1 illustrates how lead field vectors vanish in the case of sources located directly below the sensor, whereas for gradiometers, the sum of these lead field vectors is maximal at the sensor. Also shown in Figure 3 are detailed views of each cortical lead field directly underneath the sensor. Whereas EEG is sensitive to cortical sources located either on the banks of sulci or on the crowns of gyri, MEG lead fields decline to very low levels on the crowns of gyri and fundi of sulci.

Figure 3 shows the magnitude of the cortical lead fields for an example sensor in each of the measurement modalities. Lead fields also have signs, in the sense that a given dipole directed toward the local cortical surface may produce a positive or a negative signal at the target sensor, depending upon its orientation relative to the sensor. The signed cortical lead fields for example sensors in the different modalities are shown in Figure 4 (the same example sensors are used as in figure 3).

Figure 4 goes about here.

Orientation Cancellation

A striking difference between the EEG and MEG lead fields is that EEG sources pointing toward the local cortical surface tend to all contribute signals of the same sign to a given sensor, whereas MEG sources tend to be balanced between the two polarities. Consequently, widespread synchronous brain activity would tend to cancel more in its superposition across multiple dipoles to produce the MEG signal, and it would tend to summate more in its superposition across multiple dipoles to produce the EEG signal. This phenomenon was quantified by calculating the means and standard deviations of the OCI as follows. In the first step, the mean OCI was computed in each subject across sensors for each modality. In the second step, the means and standard deviations of these means across subjects were calculated. For referential EEG, the values of the latter were found to be 0.29 ± 0.02 , for bipolar EEG 0.38 ± 0.01 , for Laplacian EEG 0.50 ± 0.01 , for magnetometer MEG 0.88 ± 0.002 , and for gradiometer MEG 0.89 ± 0.002 . To test if these means are equal, a one-way ANOVA with fixed effects was performed (Brecht 1984; Woodward 1990). For each modality, the mean OCI was found to be statistically different from the mean OCI of every other modality ($p < 0.0001$; see supplementary table 1).

Figure 5 displays sensor-space topography plots where averages of the OCI for each sensor across subjects are mapped for each measurement modality on a two-dimensional, simplified representation of the scalp. For all three EEG derivations, OCI values are slightly larger over the right hemisphere but are relatively

uniform across the head compared to MEG. Specifically, MEG sensors located below the brain (see the arrangement of the sensors in Figure 2) have comparatively smaller OCI values. Presumably this arises from the fact that MEG sensors on the bottom row record primarily from dipoles on the ventral surface of the cortex which are not cancelled by even more ventral sources. By comparison, the rest of the MEG sensors are positioned to record from brain regions that have more symmetric cancellation patterns.

Figure 5 goes about here.

Global Sensitivity

Figure 6 depicts the global sensitivities of EEG and MEG, averaged across all subjects and sensors for a given modality and derivation. Whereas Figure 3 displays examples of cortical lead fields for only one subject and one sensor per modality, and thus allows the focality of the lead fields to be compared across example sensors, Figure 6 displays the overall sensitivity of all the sensors, and thus shows the parts of the cortex accessible to different modalities. EEG, especially referential derivations, has more homogeneous global lead fields than MEG, due to its relative sensitivity to deep sources and to dipoles of all orientations. This is especially apparent in the deep midline sources where MEG, and especially gradiometers, show low global sensitivity. These observations are further explored in Figure 7.

Figure 6 goes about here.

In Figure 7A, the GSI measure for each measurement modality is plotted as the probability distribution function (PDF) across cortical dipoles, after normalizing each dipole's contribution and representing it as a percentage of the maximum GSI value over the entire cortex for that modality and derivation. The peak values and shapes of the distributions are both of interest. The EEG distributions are narrower than those of MEG, indicating that EEG has more uniform sensitivity across the cortical surface, as noted above. The peaks of these distributions correspond to the median GSI value for each modality, and thus are smaller for more focal derivations within each modality. These observations were tested statistically in two analyses. In the first of these, for each modality and subject, the mean GSI across all dipoles was calculated for each modality and subject. The across-subject mean and standard deviation of these two quantities were $47\% \pm 4\%$ of the maximum GSI for referential EEG, $40\% \pm 4\%$ for bipolar EEG, $30\% \pm 2\%$ for Laplacian EEG, $44\% \pm 2\%$ for magnetometer MEG and $34\% \pm 5\%$ for gradiometer MEG. A one-way ANOVA (Brecht 1984; Woodward 1990) found that the differences in the mean GSI between modalities, between any two EEG derivations, and between MEG derivations, were all significant ($p < 0.0001$; see supplementary table 2).

In the second analysis, the standard deviation of the GSI was calculated for each modality, across all dipoles within each subject. The mean across subjects of these within-subject standard deviations were found to be 12% of the maximum GSI for referential EEG, 15% for bipolar EEG, 16% for Laplacian EEG, 20% for magnetometer MEG and 19% for gradiometer MEG. A one-way ANOVA showed that the values for EEG were in all cases less than those for MEG ($p < 0.01$; see supplementary table 3).

Figure 7B explores the GSI associated with seven representative cortical regions automatically parcellated by FreeSurfer. As expected based on Figure 7A, the global sensitivity of EEG is very similar across regions, whereas MEG changes by a factor of about three. For referential EEG, for example, the mean GSI as percentage of the maximum GSI on the cortex is never lower than 45% or higher than 50%. Similarly, for bipolar EEG the range is 35% to 40%, while for Laplacian EEG it is 30% to 35%. By comparison, differences are far more dramatic in the case of MEG. Specifically, superficial structures with many tangential dipoles such as the pre- and post-central gyri have high GSI, whereas deep structures with many radial dipoles such as the cingulate and para-hippocampal gyri have low GSI. Nevertheless, because magnetometers are more sensitive to deep sources (as illustrated also in Figure 6), the global sensitivities of magnetometers to these gyri is almost twice as high as that of gradiometers. By the global sensitivity measure, MEG is superior to EEG (in all derivations) when recording from the pre- and post-central gyri, but inferior to EEG when recording from deeper structures such as the fusiform, para-hippocampal and cingulate gyri. The two techniques have comparable global sensitivities when recording from the inferior frontal gyrus *pars triangularis* or from the middle temporal gyrus.

Figure 7 goes about here.

Effect of CSF layer on the Sensor Sensitivity Area (SSA)

SSA was the main measure used to quantify the focality of the lead fields in the different modalities and derivations. Figure 8 shows the SSA curves calculated for different models, modalities, and derivations. Lower curves indicate more focal measurements. We first evaluated if it was necessary to include the subcranial CSF layer in order to accurately estimate SSA for EEG, as shown in figures 8A using an analytic solution, and 8B using a realistic BEM model. Figure 8A shows the results of simulations using the analytic forward model consisting of 4 concentric spheres: brain, CSF, skull and scalp. The surface of the brain sphere is covered with radial dipoles. The vertical line in Figure 8A1 marks 25% of maximal dipole amplitude. Its intersections with the green and blue curves indicate the cortical area with dipoles whose amplitudes are at least that strong, for the models without, or with CSF, respectively. Thus, the total area with dipoles of signal vector strengths greater than 25% of the largest vector strength among all dipoles comprises ~25% of the sphere when CSF is included, and ~5% when it is omitted. The log-log plot in figure 8A2 shows that the decrease in focality when CSF is omitted extends to all thresholds x . The ratio curve (Figure 8A3) shows that ~3.5 to ~5 times more cortical area is involved in projecting to a particular sensor if CSF is included in the model.

Comparison of SSA for MEG and EEG in different derivations

These effects of including a subcranial CSF layer are replicated in Figure 8B using a realistic BEM model with the CSF, skull and scalp surfaces derived from the structural MRIs of the same 7 subjects. Forward solutions were calculated for ~300,000 dipoles tiling the reconstructed cortical surface in each subject. The SSA curves to the realistic model are similar to those generated by the analytical model, except that the curves in the realistic calculations include larger areas with small contributions, probably reflecting the inclusion of deep cortex far from the sensors in the realistic model. The calculations shown in Figure 8B1 confirm that the inclusion of CSF results in EEG cortical lead fields that are considerably less focal than when it is omitted. Again, Figure 8B2 shows that these differences hold across a wide range of thresholds x . In this realistic simulation, the effects of including CSF are larger, with about an eightfold increase in the size of the contributing cortical area at $x = 25\%$ (Figure 8B3). The relative increase in SSA is greatest for $x \approx 37\%$, where the increase is ~23-fold for referential EEG. Figure 8B also shows that including CSF has similar effects in reducing the focality of the forward projections when the EEG is recorded bipolarly.

The curves in Figure 8C compare the SSA measure for different measurement modalities and derivations. Whereas Figure 3 shows examples of lead fields for different measures, Figure 8C attempts to quantify their focality. Figure 8C1 shows that, consistent with Figure 3, the focality of gradiometers is highest, whereas that of referential EEG is lowest. The focality of magnetometers is inferior to that of gradiometers but superior to that of referential or bipolar EEG. Magnetometer MEG is more focal than Laplacian EEG for $\sim 3\% < x < \sim 40\%$, and their positions reverse with Laplacian EEG more focal at other values of x . The focalities of Laplacian and bipolar EEG are higher than that of referential EEG, though not as high as that of MEG gradiometers.

We also calculated the half-sensitivity area, to allow our values to be compared to Srinivasan (Srinivasan 2007). In our plots, this can be derived by measuring where the vertical line at $x = 50\%$ intersects the SSA curves, followed by a transform from percent of cortical area to cm^2 . The HSA we find for gradiometers is 6 cm^2 , for magnetometers 48 cm^2 , for Laplacian EEG 44 cm^2 , for bipolar EEG 105 cm^2 , and for referential EEG 147 cm^2 . Thus, by this measure, planar magnetometers are about 25 fold more focal than referential EEG. Figure 8C2 shows not only that the greater focality of gradiometers applies across multiple thresholds, but also that it shows characteristic differences at different values of x .

As shown in Figure 8C3, the SSA's for different modalities and derivations are all several fold greater than those of gradiometers. The peak ratio of the cortical area projecting with a given minimal strength x is up to 8 to 30-fold larger for all modalities and derivations compared to gradiometers. This focality advantage of gradiometer MEG compared to EEG applies to all values of x . Magnetometer MEG is also more focal than either referential or bipolar EEG, but again, it is more focal than Laplacian EEG only for $\sim 3\% < x < \sim 40\%$. With this partial exception, MEG is more focal than EEG. This difference is most extreme in the comparison of gradiometers to referential EEG.

Figure 8 goes about here.

Figure 9A presents the empirical probability distribution functions (PDF's) of lead field magnitudes for each modality and derivation, as computed over all sources, sensors and subjects. The peak of each curve indicates the most frequently encountered dipole contribution relative to the maximally projecting dipole (i.e., the

'normalized projection strength'). This contribution is 0.8% for gradiometers, 2.5% for magnetometers, 5% for Laplacian EEG, 9% for bipolar EEG and 16% for referential EEG. Thus, the most common normalized projection strength of referential EEG is roughly 20 times larger than that of gradiometers. This 'background contribution' to EEG sensors is apparent also in the diffuse low level red shading of the brains in the top row of Figure 3. Other modalities and measurements fall between these extremes, in the same order as other comparisons.

In Figure 9B, histograms of the cortical lead field focality measure F are shown for MEG and EEG, again computed over all sensors and subjects. This measure is equal to the mean cortical lead field magnitude normalized by the maximum magnitude. This measure denotes the average contribution of each source to the signal recorded at the sensor. The peaks of the curves in Figure 9B are further to the right than the peaks in Figure 9A, because in 9B the average is taken over all dipoles before calculating the PDF. To understand the difference between these curves, consider the most commonly occurring instances plotted for the gradiometers, indicated by the peaks of the dashed red lines. Whereas the normalized projection strength of the most commonly occurring dipole is ~0.8% (Figure 9A), the average normalized projection strength across all of the dipoles projecting to a given sensor is ~3% (Figure 9B), because it also includes the more strongly contributing dipoles. The most common F value for magnetometers was 4%, for Laplacian EEG 6%, for bipolar EEG 9% and for referential EEG 18.5%. Thus, this measure is consistent with SSA in indicating that same order of focality: gradiometer MEG, magnetometer MEG, Laplacian EEG, bipolar EEG and referential EEG.

Figure 9 goes about here.

Effect of MEG sensor distance from the scalp on the SSA

Figure 10 documents the dependence of the SSA measure upon the distance d from sensor to scalp for the sample sensor shown in part A. Five curves are shown, for distances of 1, 2, 3, 4 or 5 cm. As expected, magnetometers (Figure 10B1) are less focal than gradiometers (Figure 10C1) at all values of d . Figures 10B3 and 10C3 illustrate how the maximum SSA roughly doubles when the distance of the sensor from the scalp increases from 1 to 2 cm, and then doubles again when the distance increases from 2 to 3 cm. Above this range (i.e. when d increases from 4 cm to 5 cm), the maximum SSA value increases by about 30% for magnetometers and by about 60% for gradiometers. The decrease in focality for gradiometers from 1 cm to 5 cm is similar in magnitude to that from gradiometers to magnetometers or Laplacian derivations, in the standard sensor locations.

Figure 10 goes about here.

Discussion

In this study, EEG and MEG cortical lead fields were calculated using realistic BEM forward models with four compartments (including the subcranial CSF), and detailed cortical reconstructions with ~300,000 dipoles perpendicular to the local surface. Four measures, namely *global sensitivity index (GSI)*, *sensor sensitivity area (SSA)*, *focality (F)* and *orientation cancellation index (OCI)* were used to quantify and compare the lead fields of EEG and MEG. Three common EEG montages (referential, bipolar, Laplacian) and two MEG modalities (magnetometer and planar gradiometer) were investigated. Gradiometer MEG lead fields were clearly more focal than those of the other techniques, whereas referential EEG was found to be least focal. Though thin, the subcranial CSF layer was found to significantly reduce EEG focality in both analytic and realistic models. Magnetometers were confirmed to be insensitive to sources located directly underneath the sensor, where gradiometer sensitivity is maximal. MEG focality was found to be highly dependent upon source-to-sensor separation. EEG lead fields tend to be consistently oriented relative to the cortical surface, whereas MEG lead fields are more balanced between the two polarities resulting in greater cancellation of distributed sources. MEG was relatively insensitive to radial sources at gyral crowns, and to deep sources, whereas EEG's global sensitivity was found to be largely uniform across the cortex. The quantitative differences in the focality of gradiometer MEG versus referential EEG lead fields are sufficiently strong as to imply qualitative differences in how these recordings can be interpreted with respect to their underlying neural substrates.

This study is the first to compare EEG and MEG lead fields using a detailed cortical reconstruction, as well as anatomically correct modeling of the head including the subcranial CSF layer. Previous studies have indicated that this CSF layer has a large effect on the EEG forward solution due to its high conductivity (Ramon

2007; Ramon 2004). As current travels from its cortical generators to the scalp EEG sensors, the intervening tissues, and especially the skull and subcranial CSF, act as a spatial smearing filter, distributing the contribution of each dipole across large areas of the scalp (Bangera 2010). Previous studies of EEG and MEG lead fields by Malmivuo et al (Malmivuo 1997) and Srinivasan et al. (Srinivasan 2007) used models which did not include a subcranial CSF layer. Nunez and Srinivasan (Nunez 2006) offered simulations using a spherical shell model showing that the effects of the CSF layer on the overall scalp amplitude produced by cortical dipoles could be accounted for by modifying the brain:skull conductivity ratio. Their results suggest that, unless the source is very close to the innermost shell, the addition of a CSF layer to a three-sphere model has only a minor effect upon lead field focality and upon scalp potential amplitude. In contrast, detailed calculations by Wendel et al. using a 4-sphere model (Wendel 2008) found that the half-sensitivity volume (HSV) of bipolar electrode pairs in the 10-20 montage is more than twice as large in the 4-sphere than in the 3-sphere model. When using a realistic FEM model of the head, Wendel et al. found that inclusion of the CSF increases the HSV by a factor of ~ 2 . These authors' results also suggest that the maximum scalp amplitude due to a single dipole is more than twice as high in the CSF-exclusive as in the CSF-inclusive case. Similarly, Ramon et al. (Ramon 2006a; Ramon 2004; Ramon 2006b) reported that the maximum scalp potential due to a radial dipole is more than two times larger in their CSF-exclusive, realistic FEM model than in their CSF-inclusive model. They also found that the range and standard deviation of scalp potentials are more than twice as large when the subcranial CSF layer is included. We found similar effects when we plotted our data in the same manner as done by Nunez and Srinivasan (Nunez 2006) (please see Supplementary Figure 1). The values we calculated for the HSA were even more divergent from those reported by Srinivasan et al. (Srinivasan 2007). For example, we calculated the HSA for referential EEG to be 147 cm^2 , over ten times larger than the 13 cm^2 calculated by Srinivasan et al. (Srinivasan 2007). This difference appears to result from inclusion of the subcranial CSF layer because we obtain similar values to Srinivasan when that layer is omitted (please see the ratio curves in Figure 8B3). An additional difference between our studies is that they modeled the head volumes for the forward solution using ellipsoids, whereas we used anatomically correct BEM surfaces extracted from each subject's MRI. Although anatomically accurate geometries in the head model may result in more accurate forward solutions (Buchner 1995; Meijs 1989; Meijs, et al. 1987; Mosher 1999c; Stok, et al. 1986), the differences are not large enough to be the reason for our divergent results. Although our 4-shell BEM forward model was more anatomically accurate than that used in these previous studies, it still contained known inaccuracies that may have affected our results. Specifically, our approach did not take into account the known anisotropy of brain conductance (especially due to the orientation of white matter fibers), nor that of the skull (which comprises two layers of compact bone separated by the dipole with higher conductance). In addition, our anatomical model ignores the effects of sutures, or foramina in the skull. Finally, our cortical source space is inaccurate in that it includes non-cortical structures such as the thalamus and corpus callosum. These shortcomings can be significant because skull defects affect the distribution as well as amplitude of scalp potentials (Li 2007). Skull anisotropy can also produce significant effects, and although our conductivity ratios are standard in the field (Baumann 1997; Geddes 1967), tissue conductivities (such as that of bone) are not only difficult to measure *in vivo* but also variable within and across subjects. Nevertheless, previous work with more realistic models indicates that omitting anisotropy from forward solutions does not usually have a very large effect on potential or field topographies, or on the source distributions estimated based on these forward solutions (Haueisen 2002; Wolters 2006; Zhou 1992).

Another critical issue in calculation of cortical lead fields is the accuracy of the cortical representation. Because the currents giving rise to the MEG are mainly within the apical dendrites of cortical pyramidal cells, the source dipoles are perpendicular to the local cortical surface. The projections of such dipoles to the MEG sensors are highly dependent on their orientations (Cuffin 1979). At the limit, radially-oriented sources located within a sphere do not produce a signal external to the sphere (Sarvas 1987). Thus, correct forward modeling requires accurate representation of cortical dipole orientations, and given the high curvature of the cortex, especially at sulcal fundi and gyral crowns, this requires high resolution tessellation. We used a tessellation with $\sim 300,000$ dipoles, resulting in an average inter-vertex spacing of $\sim 1 \text{ mm}$. We found that lower resolution tessellations degraded our results because they could not accurately capture sensitivity changes in areas of large curvature. A similar conclusion and similar accuracy were used by Hillebrand & Barnes (Hillebrand 2002), who also mapped the sensitivity of MEG to different locations on the cortical surface. Unlike our study, they used a spherical rather than realistic head model, radial rather than planar gradiometers, and two rather than seven subjects. They did not examine the cortical sensitivity of EEG. Further, their measure of MEG sensitivity was the probability of detecting sources with an inverse solution, rather than the root mean square of the

forward solution. Nonetheless, their major results are consistent with ours. First, they found thin strips about 2 mm wide on the gyral crowns and sulcal fundi of external cortex where MEG has low sensitivity, consistent with the radial orientation of dipoles in these locations. However, much larger areas of relatively low sensitivity to MEG were in deep cortical locations far from the scalp. Our study confirmed both of these findings using a different forward solution and measure of sensitivity, as well as more subjects. For example, by our measure, gradiometers are over three times less sensitive to activity in cingulate cortex than in the precentral gyrus, whereas EEG is equally sensitive. Nonetheless, it should be noted that the insensitivity of MEG to deep sources is only relative to its sensitivity to superficial sources, and to EEG's sensitivity to deep sources. The literature contains numerous convincing theoretical treatments (Hamalainen 1989) and empirical examples (Halgren 2000) showing that MEG can detect deep sources.

The major finding of this study is that MEG cortical lead fields are generally more focal than EEG, and in particular, gradiometer lead fields are more focal than referential EEG. The only partial exception to this pattern was that the Laplacian EEG derivation was comparable in focality to MEG magnetometers. This finding suggests that this derivation should be used more commonly, provided that technical challenges can be addressed. These challenges include the increased noise in subtractions as compared to the original recordings, the greater dependence on identical amplifier characteristics and exact knowledge of electrode location, and most importantly, the need for a very accurate forward solution including local characteristics of the skull which might produce small differences between adjacent EEG leads (e.g., sutures, foramina, and the thickness of the inner and outer tables and diploe, and CSF layer). Conversely, it is important to note that the focality of MEG is strongly dependent on the distance of the MEG sensor to the cortical source. For example, the focality of MEG recordings drops about six fold as the sensor moves from 1 cm to 5 cm away from the scalp. This may be a significant factor in populations (e.g. infants) where achieving optimal head position is difficult to accomplish.

In addition to their lower focality, EEG lead fields differ from MEG in the consistency of their orientation relative to the local cortical surface. We quantified this difference by finding the ratio of the sum of the signed forward matrix elements associated with a given sensor, to the sum of their absolute values. One minus this value is termed the Orientation Cancellation Index (OCI). The OCI was ~ 0.3 for referential EEG and ~ 0.9 for gradiometers. This means that only about 30% of the average referential EEG signal would be lost to cancellation if its entire cortical lead field were to be uniformly active, whereas $\sim 90\%$ of the gradiometer signal would be lost. This property of EEG, compounded with its large lead fields, makes it much more sensitive than MEG to widespread synchronous cortical activity. Ahlfors et al. (Ahlfors 2009) also found that cortical activity is cancelled less by non-uniformity of source orientations for EEG than MEG. Although our results are globally consistent, we found greater differences between EEG and MEG because we examined the situation when the entire lead field is active, whereas they used a limited patch; and we used a four shell BEM forward model whereas they used three shells.

We found that the Sensor Sensitivity Area (SSA) for gradiometers was about 25 times smaller than that of referential EEG at 50% of maximum (HSA). This large difference has important consequences for the properties of the signals recorded by these modalities. First, as noted by Srinivasan et al. (Srinivasan 2007), coherence between signals recorded by different sensors can reflect either coherence in neural oscillations between different brain regions, or crosstalk between those sensors. The former possibility is interpreted as implying functional linkage between brain areas, but the later possibility is highly likely when there is substantial overlap in the lead fields of the sensors. The lead fields for referential EEG found in the current study (Figure 3) are sufficiently large that any two sensors will have substantial overlap, and thus any coherence between referential EEG signals may arise from sensor crosstalk. Even in the case of the Laplacian montage, which generally offers higher spatial resolution than both referential and bipolar EEG, the cortical area giving rise to the signal recorded at a single location may include large areas of both hemispheres. Consistent with Srinivasan et al. (Srinivasan 2007), our studies indicate that magnetometer recordings are more restricted spatially than EEG, but still can reflect the activity in large areas and so coherence between magnetometer signals still need to be interpreted with caution. In contrast, we found that the gradiometer lead fields are localized to a relatively small region directly beneath the sensor, and thus it is quite practical to choose pairs of sensors whose lead fields do not overlap. In these circumstances, coherence between planar gradiometer signals can be strongly interpreted as coherence between the underlying cortical areas. Such inferences need to be strongly qualified for EEG and magnetometer recordings by the possibility of crosstalk. We did not analyze radial gradiometers.

The fact that gradiometer lead fields are generally limited to the directly underlying cortex also allows them to be used to validate inferences from mathematical source localization procedures. The large lead field of EEG sensors does not prevent highly accurate localization of sources that are known *a priori* to be single dipoles. Indeed, both theoretical and empirical studies indicate that the accuracy of single dipole localization is comparable for EEG and MEG (Cohen 1990; Cuffin 1986; Cuffin 1990; Leahy 1998; Liu 2002; Mosher 1993; Murro 1995; Stok 1987). It should be noted that theoretical studies seldom included the subcranial CSF layer which we showed here to be important (Cuffin 1986; Cuffin 1990), and that most assumed a perfect forward solution (Mosher 1993; Murro 1995; Stok 1987). This limitation does not apply to studies where artificial dipoles were placed in a phantom (Leahy 1998) or living brain (Cohen 1990), and localization from EEG or MEG measurements yielded comparable errors from the actual positions. However, cortical activity to sensory stimulation spreads to multiple areas within about 15 ms of onset, before 40 ms to auditory and somatosensory stimuli, and before 80 ms to visual. Thus, the circumstances where focal generation can be assumed may be very limited. Furthermore, direct intracranial recordings indicate that cognitive evoked fields, of greatest interest in humans, are generated by extended generators in multiple areas (Halgren 1994; Halgren 2002).

When multiple distributed generators are co-active then the high levels of cross-talk between cortical sources pose great challenges for inverse estimates. Consider, for example, the N400, evoked by words and modulated by semantic priming. In the referential EEG, the N400 is maximal over the centroparietal regions (Johnson 2000). In Laplacian derivations, the N400 is very difficult to discern (Curran 1993). Single dipole localization of the N400 recorded with MEG placed its generator in the left posterior superior temporal sulcus (Helenius 1998). A noise-normalized cortically-constrained minimum norm inverse procedure, with or without fMRI bias, estimated sources in Wernicke's and Broca's regions, as well as the anteroventral temporal lobe (Dale 2000; Halgren 2002). There is a comparable lack of consistency between the various inverse estimates proposed for the P300 cognitive potential or its MEG homologue (Halgren 2008). These differences between inverse estimates are presumed to mainly reflect their different assumptions, such as the number of sources generating the signal, how extended those sources are, and whether the sources are allowed to be correlated. Extensive intracranial recordings permit us to select the correct inverse solutions for the N400 and P300 (Halgren 2004). However, in general, such recordings are not available. In these cases, the focality of gradiometer lead fields allows sources to be inferred without performing a mathematical inverse procedure. Specifically, activity recorded by a sensor can be directly inferred to be generated by sources active in its cortical lead field. We show here that the lead fields of MEG gradiometers are generally sufficiently focal that one can directly infer that the activity they record is arising in the underlying cortex, without application of an inverse solution with its attendant assumptions (Halgren 2010). In contrast, the cortical lead fields of EEG are too large for such inferences to be of value.

The large quantitative differences between gradiometers and referential EEG may even interact with the underlying neurobiology of synchronous cortical activity to result in qualitative differences in the neural systems that they record. For example, spindle activity simultaneously recorded by MEG and EEG during stage 2 NREM sleep are poorly related: MEG spindles and EEG spindles often occur independently of each other, and when they do occur together they are asynchronous and incoherent (Dehghani 2010a; Dehghani 2010b). Since spindles are known to arise in thalamocortical oscillations (Destexhe 2003), and there are two major thalamocortical systems (Jones 2001), one explanation for these striking dissociations is that gradiometers and referential EEG are differentially sensitive to these systems due to their different biophysics. Indeed, the core thalamocortical system has focal projections with large boutons suggesting that it supports focal and asynchronous but strong activity, whereas the matrix thalamocortical system has diffuse projections with small presynaptic boutons suggesting that it supports distributed synchronous but weak activity (Zikopoulos 2007). Gradiometers, with small lead fields (small SSA) and high cancellation (high OCI) would be strongly biased toward the focal sources activated by core afferents, whereas referential EEG, with large lead fields (large SSA) oriented consistently (and thus low OCI), would be strongly biased to recording diffuse synchronous activity from the matrix. Note that in this case, the differences between MEG and EEG permit a greater range of physiological phenomena to be recorded than is available to either technique alone. Although MEG offers better spatial resolution, it comes at the price of relative insensitivity to global processes easily detected by EEG. More generally, a deep appreciation of the cortical lead fields of EEG and MEG are crucial for a biologically-based understanding of the signals they record.

Acknowledgments

This work was supported by the National Institutes of Health (R01-EB 09282, R01-NS 18741 to A.I. and E.H., R01-NS 47293 to Z. A. A., and K01-MH 79146 to D. J. H.); the Schwartz Foundation (to Z. A. A.); and the Department of Veterans' Affairs (051455 and 060812 to M. X. H.). We gratefully acknowledge Maxim Bazhenov, Timothy T. Brown, Sydney S. Cash, Gaute T. Einevoll, Matthew K. Leonard, Ksenija Marinković, Carrie R. McDonald, Terrence J. Sejnowski, Jason S. Sherfey and Katherine E. Travis for useful discussions and comments. Correspondence should be addressed to Andrei Irimia, Ph.D., Multimodal Imaging Laboratory, University of California, San Diego, 9500 Gilman Drive #0841, La Jolla, CA 92037, USA.

References

- Ahlfors SP, Han, J., Lin, F.S., Witzel, T., Belliveau, J.W., Hamalainen, M.S., Halgren, E. 2009. Cancellation of EEG and MEG signals generated by extended and distributed sources. *Human Brain Mapping*.
- Akalin-Acar Z, Gencer, N.G. 2004. An advanced boundary element method (BEM) implementation for the forward problem of electromagnetic source imaging. *Physics in Medicine and Biology* 49:5011-5028.
- Akalin-Acar Z, Makeig, S. 2008. Neuroelectromagnetic forward modeling toolbox. *IEEE Engineering in Medicine and Biology Conference*. Vancouver, BC, Canada: IEEE.
- Akalin-Acar Z, Makeig, S. 2010. Neuroelectromagnetic forward head modeling toolbox. *Journal of Neuroscience Methods* 190:258-270.
- Bangera NB, Schomer, D.L., Dehghani, N., Ulbert, I., Cash, S., Papavasiliou, S., Eisenberg, S.R., Dale, A.M., Halgren, E. 2010. Experimental validation of the influence of white matter anisotropy on the intracranial EEG forward solution. *Journal of Computational Neuroscience* in press.
- Baumann S, Wozny, D., Kelly, S., Meno, F. 1997. The electrical conductivity of human cerebrospinal fluid at body temperature. *IEEE Transactions on Biomedical Engineering* 44(3):220-223.
- Berg P, Scherg, M. 1994. A fast method for forward computation of multiple-shell spherical head models. *Electroencephalography and Clinical Neurophysiology* 90(1):58-64.
- Brecht ML, Woodward, J.A. 1984. GANOVA: a univariate/multivariate analysis of variance program for the personal computer. *Educational and Psychological Measurement* 44:169-173.
- Buchner H, Waberski, T.D., Fuchs M., Wischmann H.A., Wagner M., Drenckhahn R. 1995. Comparison of realistically shaped boundary-element and spherical head models in source localization of early somatosensory evoked potentials. *Brain Topography* 8(2):137-143.
- Cohen D, Cuffin, B.N., Yunokuchi, K., Maniewski, R., Purcell, C., Cosgrove, G.R., Ives, J., Kennedy, J.G., Schomer, D.L. 1990. MEG versus EEG localization test using implanted sources in the human brain. *Annals of Neurology* 28:811-817.
- Cuffin BN. 1986. Effects of measurement errors and noise on MEG moving dipole inverse solutions. *IEEE Transactions on Biomedical Engineering* BME-33:854-861.
- Cuffin BN. 1990. Effects of head shape on EEG's and MEG's. *IEEE Transactions on Biomedical Engineering* 37:44-52.
- Cuffin BN, Cohen, D. 1979. Comparison of the magnetoencephalogram and electroencephalogram. *Electroencephalography and Clinical Neurophysiology* 47:132-146.
- Curran T, Tucker, D.M., Kutas, M., Posner, M.I. 1993. Topography of the N400: brain electrical activity reflecting semantic expectancy. *Electroencephalography and Clinical Neurophysiology* 88:188-209.
- Dale AM, Fischl B, Sereno MI. 1999. Cortical surface-based analysis - I. Segmentation and surface reconstruction. *Neuroimage* 9(2):179-194.
- Dale AM, Halgren, E. 2001. Spatiotemporal mapping of brain activity by integration of multiple imaging modalities. *Current Opinion in Neurobiology* 11(2):202-208.
- Dale AM, Liu, A.K., Fischl, B.R., Buckner, R.L., Belliveau, J.W., Lewine, J.D., Halgren, E. 2000. Dynamic statistical parametric mapping: combining fMRI and MEG for high-resolution imaging of cortical activity. *Neuron* 26:55-67.
- Dale AM, Sereno MI. 1993. Improved Localization of Cortical Activity by Combining EEG and MEG with MRI Cortical Surface Reconstruction - a Linear-Approach. *Journal of Cognitive Neuroscience* 5(2):162-176.
- de Munck JC, Hamalainen, M.S., Peters, M.J. 1991. The use of the asymptotic expansion to speed up the computation of a series of spherical harmonics. *Clinical Physiology and Measurement* 12:83-87.
- Dehghani N, Cash, S.S., Chen, C.C., Hagler, D.J., Huang, M.X., Dale, A.M., Halgren, E. 2010a. Divergent cortical generators of MEG and EEG during human sleep spindles suggested by distributed source modeling. *PLoS One* 5:e11454.
- Dehghani N, Cash, S.S., Rossetti, A.O., Chen, C.C., Halgren, E. 2010b. Magnetoencephalography demonstrates multiple asynchronous generators during human sleep spindles. *Journal of Neurophysiology* 104:179-188.
- Destexhe A, Sejnowski, T.J. 2003. Interactions between membrane conductances underlying thalamocortical slow-wave oscillations. *Physiological Review* 83:1401-1453.
- Einevoll GT, Pettersen, K.H., Devor, A., Ulbert, I., Halgren, E., Dale, A.M. 2007. Laminar population analysis: estimating firing rates and evoked synaptic activity from multielectrode recordings in rat barrel cortex. *Journal of Neurophysiology* 97:2174-2190.

- Fischl B, et al. 2004. Automatically parcellating the human cerebral cortex. *Cerebral Cortex* 14(1):11-22.
- Fischl B, Sereno MI, Dale AM. 1999a. Cortical surface-based analysis - II: Inflation, flattening, and a surface-based coordinate system. *Neuroimage* 9(2):195-207.
- Fischl B, Sereno MI, Tootell RBH, Dale AM. 1999b. High-resolution intersubject averaging and a coordinate system for the cortical surface. *Human Brain Mapping* 8(4):272-284.
- Frijns JHM, de Snoo, S.L., Schoonhoven, R. 2000. Improving the accuracy of the boundary element method by the use of second-order interpolation functions. *IEEE Transactions on Biomedical Engineering* 47(1336-1346).
- Fuchs M, Wagner, M., Kastner, Jorn. 2001. Boundary element method volume conductor models for EEG source reconstruction. *Clinical Neurophysiology* 112:1400-1407.
- Geddes LA, Baker, L.E. 1967. Specific resistance of biological material - a compendium of data for biomedical engineer and physiologist. *Medical & Biological Engineering* 5:271.
- Halgren E. 2004. How can intracranial recordings assist MEG source localization? *Neurology and Clinical Neurophysiology* 86:1-18.
- Halgren E. 2008. Considerations in source estimation of the P3. In: Ikeda A, Inoue, Y., editor. *Event-related potentials in patients with epilepsy: from current state to future prospects*. Eshery, Surrey, UK: John Libbey Eurotext. p 71-88.
- Halgren E, Baudena, P., Heit, G., Clarke, M., Marinkovic, K. 1994. Spatiotemporal stages in face and word-processing. 1. Depth recorded potentials in the human occipital and parietal lobes. *Journal of Physiology-Paris* 88:1-50.
- Halgren E, Dhond, R.P., Christensen, N., van Petten, C., Marinkovic, K., Lewine, J.D., Dale, A.M. 2002. N400-like magnetoencephalography responses modulated by semantic context, word frequency, and lexical class in sentences. *NeuroImage* 17:1101-1116.
- Halgren E, Raji, T., Marinkovic, K., Jousmaki, V., Hari, R. 2000. Cognitive response profile of the human fusiform face area as determined by MEG. *Cerebral Cortex* 10:69-81.
- Halgren E, Sherfey, J.S., Irimia, A., Dale, A.M., Marinkovic, K. 2010. Sequential temporo-fronto-temporal activation during monitoring of the auditory environment for temporal patterns. *Human Brain Mapping* in press.
- Hamalainen M, Hari R, Ilmoniemi RJ, Knuutila J, Lounasmaa OV. 1993. Magnetoencephalography - Theory, Instrumentation, and Applications to Noninvasive Studies of the Working Human Brain. *Reviews of Modern Physics* 65(2):413-497.
- Hamalainen MS, Sarvas, J. 1989. Realistic conductivity geometry model of the human head for interpretation of neuromagnetic data. *IEEE Transactions on Biomedical Engineering* 36:165-171.
- Haueisen J, Tuch, D.S., Ramon, C., Schimpf, P.H., Wedeen, V.J., George, J.S., Belliveau, J.W. 2002. The influence of brain tissue anisotropy on human EEG and MEG. *Neuroimage* 15:159-166.
- Helenius P. 1998. Distinct time courses of word and context comprehension in the left temporal cortex. *Brian* 121:1133-1142.
- Hillebrand A, Barnes, G.R. 2002. A quantitative assessment of the sensitivity of whole-head MEG to activity in the adult human cortex. *NeuroImage* 16:638-650.
- Hjorth B. 1975. An on-line transformation of EEG scalp potentials into orthogonal source derivations. *Electroencephalography and Clinical Neurophysiology* 39:526-530.
- Jasper HH. 1974. The 10-20 electrode system of the International Federation. *Handbook of Electroencephalography and Clinical Neurophysiology*. Amsterdam: Elsevier.
- Johnson BW, Hamm, J.P. 2000. High-density mapping in an N400 paradigm: evidence for bilateral temporal lobe generators. *Clinical Neurophysiology* 111:532-545.
- Jones EG. 2001. The thalamic matrix and thalamocortical synchrony. *Trends in Neurosciences* 24:595-601.
- Laarne P, Kauppinen, P., Hyttinen, J., Malmivuo, J., Eskola, H. 1999. Effects of tissue resistivities on electroencephalogram sensitivity distribution. *Medical & Biological Engineering & Computing* 37:555-559.
- Lagerlund TD. 1999. EEG source localization (model-dependent and model-independent methods). In: Niedermeyer E, Lopes da Silva, F., editor. *Electroencephalography: basic principles, clinical applications and related fields*. Baltimore, MD: Lippincott, Williams & Wilkins. p 809-822.
- Leahy RM, Mosher, J.C., Spencer, M.E., Huang, M.X., Lewine, J.D. 1998. A study of dipole localization accuracy for MEG and EEG using a human skull phantom. *Electroencephalography and Clinical Neurophysiology* 107:159-173.
- Li J, Wang, K., Zhu, S., He, B. 2007. Effects of holes on EEG forward solutions using a realistic geometry head model. *Journal of Neural Engineering* 4:197-204.
- Liu AK, Dale, A.M., Belliveau, J.W. 2002. Monte Carlo Simulation Studies of EEG and MEG Localization Accuracy. *Human Brain Mapping* 16:47-62.
- Liu LC, Ioannides AA, Muller-Gartner HW. 1998. Bi-hemispheric study of single trial MEG signals of the human auditory cortex. *Electroencephalography and Clinical Neurophysiology* 106(1):64-78.
- Lutkenhoener B, Grave de Peralta Menendez, R. 1997. The resolution-field concept. *Electroencephalography and Clinical Neurophysiology* 102:326-334.
- Malmivuo J, Plonsey, R. 1995. *Bioelectromagnetism*. New York: Oxford University Press.
- Malmivuo JAV. 1980. Distribution of MEG detector sensitivity: an application of reciprocity. *Medical & Biological Engineering & Computing* 18:365-370.

- Malmivuo JAV, Suihko, V., Eskola, H. 1997. Sensitivity distributions of EEG and MEG measurements. *IEEE Transactions on Biomedical Engineering* 44(3):196-208.
- Meijs J, Weier, O., Peters, M.J., van Oosterom, A. 1989. On the numerical accuracy of the boundary element method. *IEEE Transactions on Biomedical Engineering* 36:1038-1049.
- Meijs JWH, Bosch FGC, Peters MJ, Dasilva FHL. 1987. On the Magnetic-Field Distribution Generated by a Dipolar Current Source Situated in a Realistically Shaped Compartment Model of the Head. *Electroencephalography and Clinical Neurophysiology* 66(3):286-298.
- Mosher JC. 1999a. Efficiently solving the EEG/MEG forward model. *International Journal of Psychophysiology* 33(1):39-39.
- Mosher JC. 1999b. Solutions to EEG/MEG inverse models. *International Journal of Psychophysiology* 33(1):39-39.
- Mosher JC, Leahy RM, Lewis PS. 1999. EEG and MEG: Forward solutions for inverse methods. *IEEE Transactions on Biomedical Engineering* 46(3):245-259.
- Mosher JC, Leahy, R.M., Lewis, P.S. 1999c. EEG and MEG: forward solutions for inverse problems. *IEEE Transactions on Biomedical Engineering* 46:1069-1077.
- Mosher JC, Spencer, M.E., Leahy, R.M., Lewis, P.S. 1993. Error bounds for EEG and MEG dipole source localization. *Electroencephalography and Clinical Neurophysiology* 86:303-321.
- Mugler JP, Brookeman, J.R. 1990. Three-dimensional magnetization-prepared rapid gradient-echo imaging (3D MP RAGE). *Magnetic Resonance in Medicine* 15:152-157.
- Murakami S, Hirose, A., Okada, Y.C. 2003. Contribution of ionic currents to magnetoencephalography (MEG) and electroencephalography (EEG) signals generated by guinea-pig CA3 slices. *Journal of Physiology* 553:975-985.
- Murakami S, Zhang, T., Hirose, A., Okada, Y.C. 2002. Physiological origins of evoked magnetic fields and extra-cellular field potentials produced by guinea-pig CA3 hippocampal slices. *Journal of Physiology* 544:237-251.
- Murro AM, Smith, J.R., King, D.W., Park, Y.D. 1995. Precision of dipole localization in a spherical volume conductor: a comparison of referential EEG, magnetoencephalography and scalp current density methods. *Brain Topography* 8:119-125.
- Nenonen J, Kajola, M., Simola, J., Ahonen, A. 2004. Total information of multichannel MEG sensor arrays. *Proceedings of the 14th International Conference on Biomagnetism (BIOMAG 2004), Boston, Massachusetts, USA*:630-631.
- Nunez PL, Srinivasan, R. 2006. *Electric fields of the brain: the neurophysics of EEG*. New York, New York: Oxford University Press.
- Ramon C, Haueisen, J., Schimpf, P.H. 2006a. Influence of head models on neuromagnetic fields and inverse source localizations. *Biomedical Engineering Online* 5:55.
- Ramon C, Haueisen, J., Schimpf, P.H. 2007. Influence of head models on neuromagnetic fields and inverse source localizations. *Biomedical Engineering Online* 5:55.
- Ramon C, Schimpf, P., Haueisen, J., Holmes, M., Ishimaru, A. 2004. Role of soft bone, CSF and gray matter in EEG simulations. *Brain Topography* 16(4):245-248.
- Ramon C, Schimpf, P., Haueisen, J., Holmes, M., Ishimaru, A. 2006b. Influence of head models on EEG simulations and inverse source localizations. *Biomedical Engineering Online*.
- Rullmann M, Anwender, A., Dannhauer, M., Warfield, S.K., Duffy, F.H., Wolters, C.H. 2009. EEG source analysis of epileptiform activity using a 1 mm anisotropic hexahedra finite element head model. *NeuroImage* 44:399-410.
- Rush S, Driscoll, D.A. 1969. EEG electrode sensitivity - an application of reciprocity. *IEEE Transactions on Biomedical Engineering* 16(1):15-22.
- Sarvas J. 1987. Basic Mathematical and Electromagnetic Concepts of the Biomagnetic Inverse Problem. *Physics in Medicine and Biology* 32(1):11-22.
- Srinivasan R, Winter, W.R., Ding, J., Nunez, P.L. 2007. EEG and MEG coherence: measures of functional connectivity at distinct spatial scales of neocortical dynamics. *Journal of Neuroscience Methods* 166:41-52.
- Stok CJ. 1987. The influence of model parameters on EEG/MEG single dipole source estimation. *IEEE Transactions on Biomedical Engineering* BME-34:289-296.
- Stok CJ, Meijs JWH, Peters MJ, Rutten WLC. 1986. Model Evaluation Using Electroencephalography and Magnetoencephalography. *Acta Oto-Laryngologica* 102:5-10.
- Wallin G, Stalberg, E. 1980. Source derivation in clinical routine EEG. *Electroencephalography and Clinical Neurophysiology* 50:282-292.
- Wendel KN, N.G., Hannula, M., Kauppinen, P., Malmivuo, J.A.V. 2008. The influence of CSF on EEG sensitivity distributions of multilayered head models. *IEEE Transactions on Biomedical Engineering* 55(4):1454-1456.
- Wolters CH, Anwender, A., Tricoche, X., Weinstein, D., Koch, M.A., MacLeod, R.S. 2006. Influence of tissue conductivity anisotropy on EEG/MEG field and return current computation in a realistic head model: a simulation and visualization study using high-resolution finite element modeling. *NeuroImage* 30:813-826.
- Woodward JA, Bonett, D.G., Brecht, M.L. 1990. *Introduction to linear models and experimental design*. San Diego, CA: Harcourt Brace Janovich.
- Yvert B, Bertrand, O., Echallier, J.F., Pernier, J. 1995. Improved forward EEG calculations using local mesh refinement of realistic head geometries. *Electroencephalography and Clinical Neurophysiology* 95:381-392.

Yvert B, Bertrand, O., Echallier, J.F., Pernier, J. 1996. Improved dipole localization using local mesh refinement of realistic head geometries: an EEG simulation study. *Electroencephalography and Clinical Neurophysiology* 99(79-89).

Yvert B, Crouzeix-Cheylus, A., Pernier, J. 2001. Fast realistic modeling in bioelectromagnetism using lead-field interpolation. *Human Brain Mapping* 14:48-63.

Zhang Z. 1995. A fast method to compute surface potentials generated by dipoles within multilayer anisotropic spheres. *Physics in Medicine and Biology* 40(3):335-349.

Zhou H, van Oosterom, A. 1992. Computation of the potential distribution in a four-layer anisotropic concentric spherical volume conductor. *IEEE Transactions on Biomedical Engineering* 39:154-158.

Zikopoulos B, Barbas, H. 2007. Parallel driving and modulatory pathways link the prefrontal cortex and thalamus. *PLoS One* 2:e848.

Figures

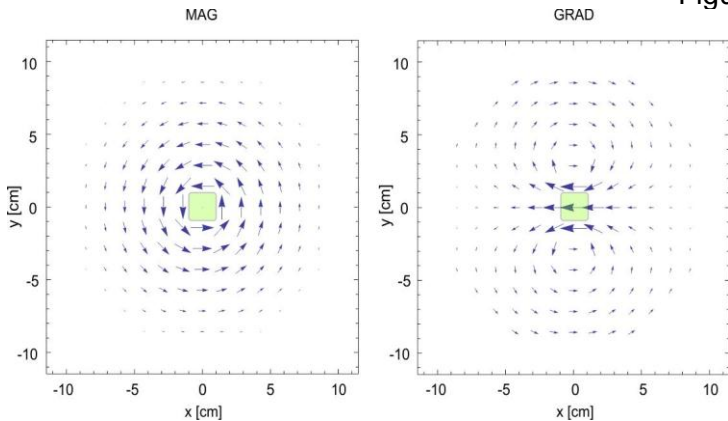


Figure 1. Lead fields of the magnetometers (MAG) and planar gradiometers (GRAD) of the Elekta Neuromag® MEG system. The square at the center of each plot represents the SQUID chip on which the MEG leads are located. Field arrow lengths are proportional to the magnitudes of the magnetic field components sampled by the array in the plane of the chip. Magnetometers are most sensitive to a ring around that sensor and blind directly underneath, where gradiometers are most sensitive.

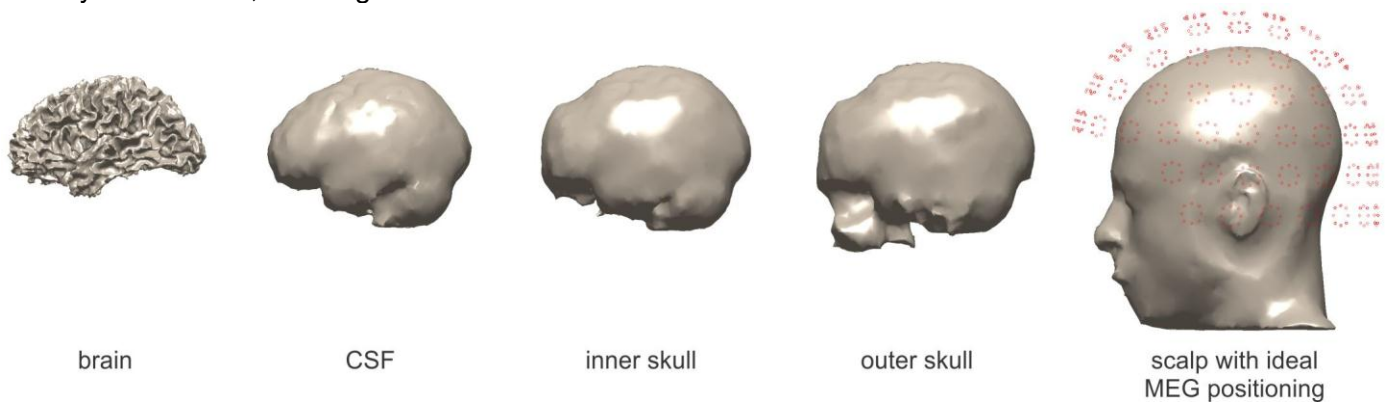


Figure 2. Sample BEM constructed from tessellated surfaces of the inner surface of the subcranial CSF volume ('CSF'), the inner-skull, outer-skull and outer-skin (scalp), as generated from the MRI of a subject in this study. The head was assumed to be positioned optimally under the MEG scanner to simulate the ideal scenario in which the distance from the recording point to the scalp is roughly the same for as many sensors as possible. Ideal sensor locations are shown in red.

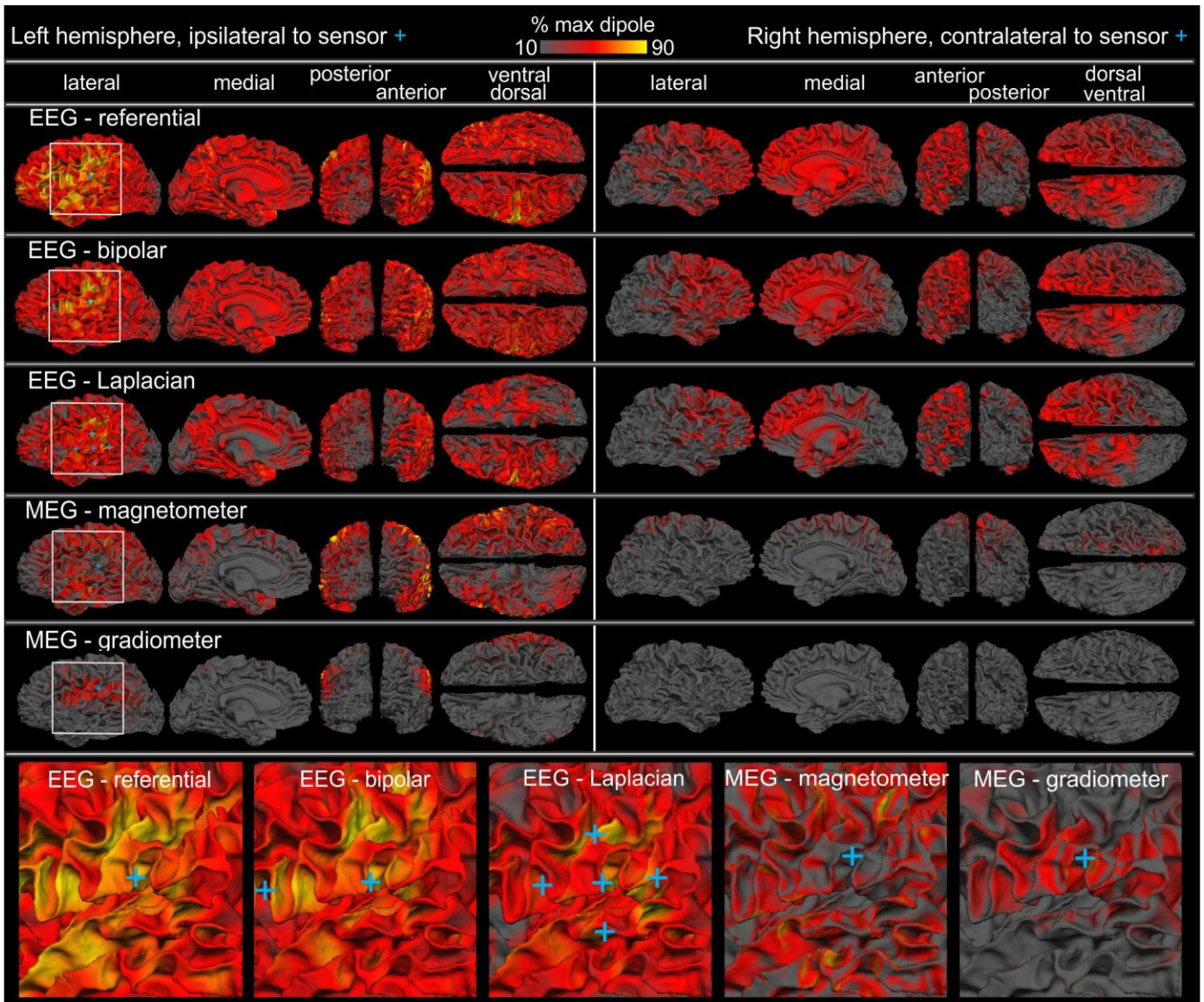


Figure 3. Examples of cortical lead fields for single referential EEG, bipolar EEG, Laplacian EEG, magnetometer MEG and gradiometer MEG sensors and derivations. Dipole contributions are normalized to the dipole contributing most strongly to that sensor, and are displayed on the white-gray interface (i.e., at the base of the cortical ribbon). Dipoles in all hemispheres of both lobes contribute to the referential EEG contact (C3). Somewhat smaller domains project to the sensors if a bipolar or Laplacian derivation is employed, but activity is still observed in both hemispheres and most lobes. Further restriction in the cortical lead fields are seen to magnetometers, with those of gradiometers concentrated almost entirely in the left frontal lobe. Detailed views of each cortical lead field for the same area of the cortex for the five modalities and derivations are shown at the bottom. As expected, sensitivity is low for sources located directly below a magnetometer, whereas for gradiometers sensitivity is maximal below such sources. In the case of MEG, regions colored in yellow (i.e. sources to which MEG is highly sensitive) may not be readily visible because they are located on the banks of sulci.

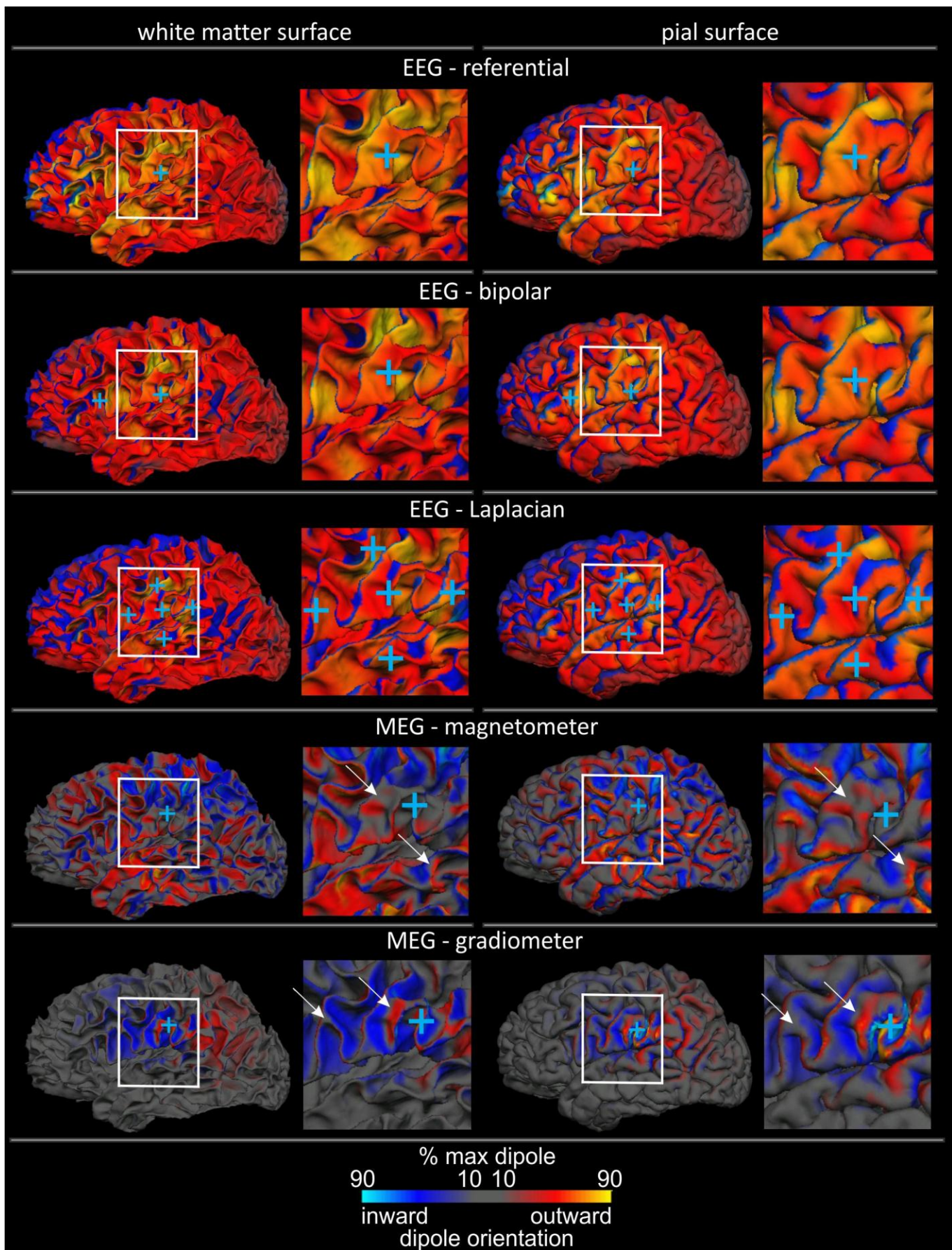


Figure 4. Lateral views of *signed* cortical lead fields. The unsigned lead fields are displayed in Figure 3. Colors indicate the direction of the dipole relative to the local cortical surface which would produce a positive signal at the sensor (red outward, i.e., away from the local white matter surface; blue inward). The EEG lead fields are

strongly biased toward dipoles pointing out of the cortex, whereas the MEG lead fields are more balanced. White arrows indicate regions of near zero sensitivity for MEG at the crowns of gyri.

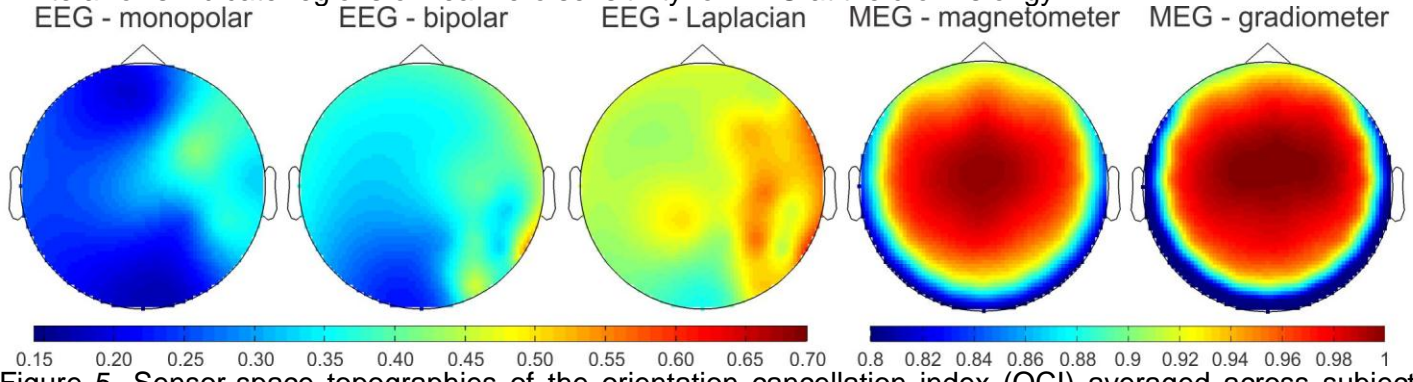


Figure 5. Sensor-space topographies of the orientation cancellation index (OCI) averaged across subjects. EEG maps are more uniform, whereas MEG topographies exhibit low OCI values for sensors located in the most ventral row (see text for details). Different color map limits are used for EEG and MEG to emphasize differences in OCI between and within modalities.

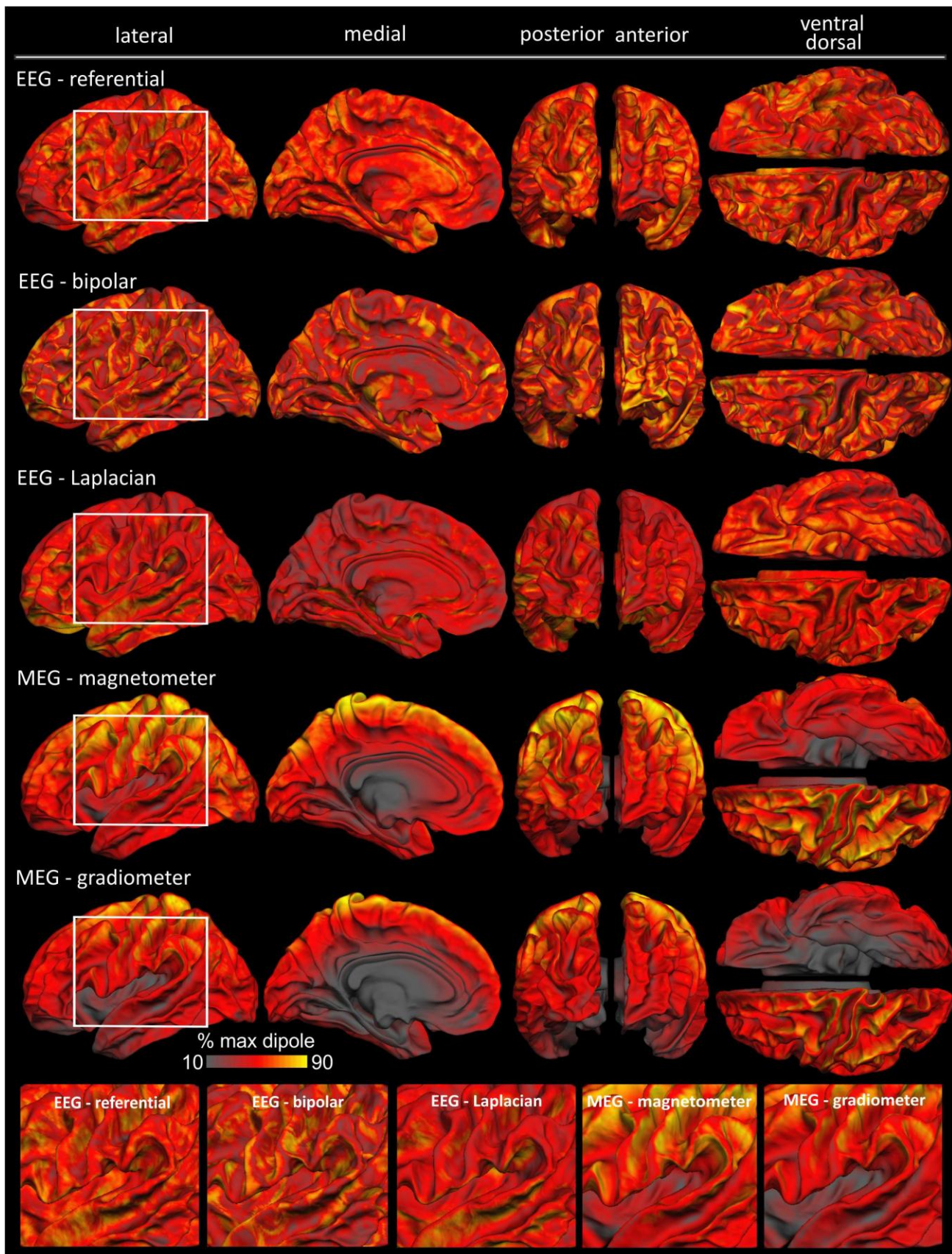


Figure 6. RMS cortical lead fields of referential EEG, bipolar EEG, Laplacian EEG, magnetometer MEG and gradiometer MEG, averaged over all sensors and all subjects in anatomic atlas space. Although only the left hemisphere is shown, the corresponding images for the right hemisphere are very similar. The color scale varies from 10% to 90% of the largest projection of any cortical dipole onto any of the sensors for a given

modality. Compared to EEG, MEG is relatively insensitive to medial and ventral cortical activity, with magnetometers more sensitive to deep sources than gradiometers.

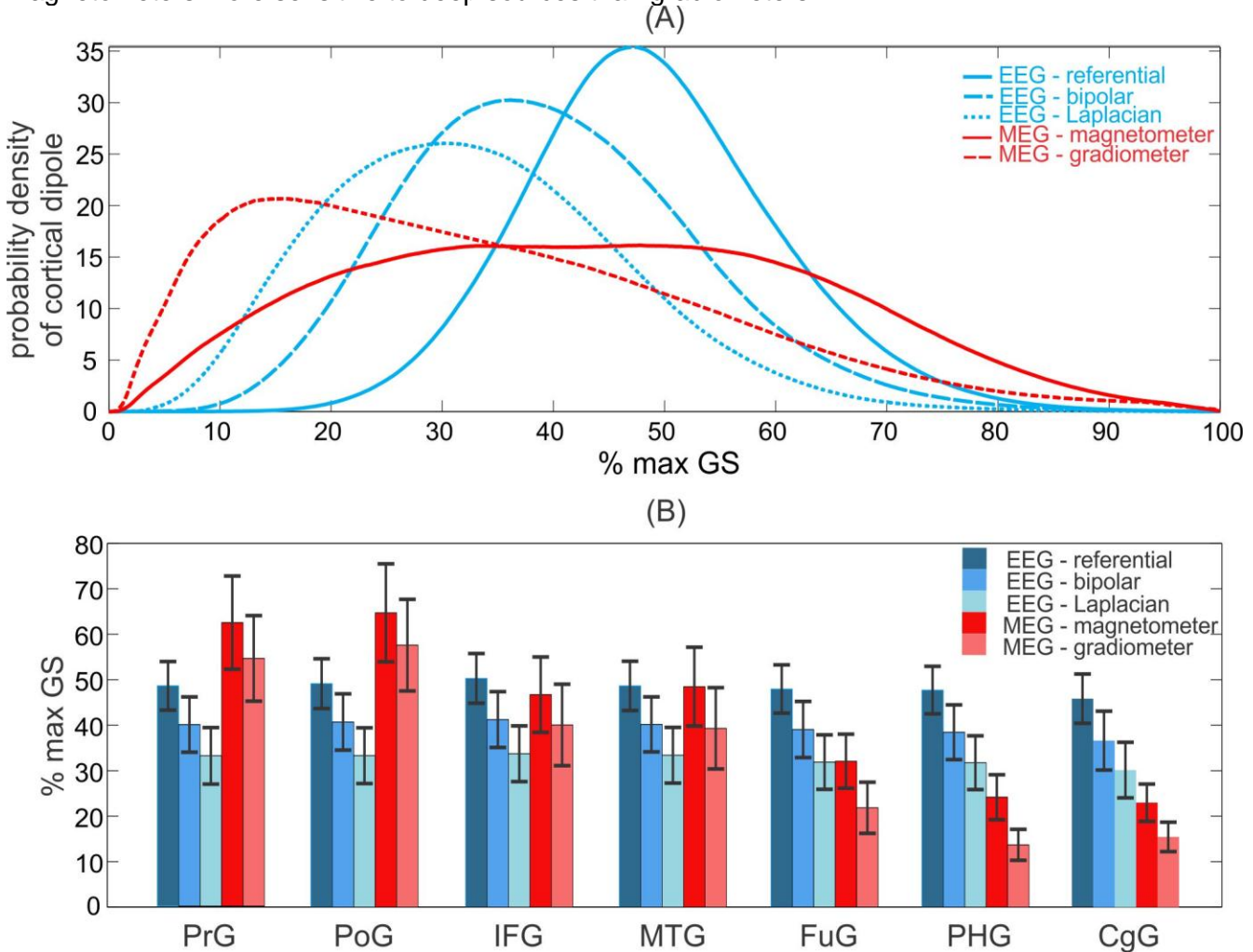


Figure 7. (A) means across subjects of the probability density functions (PDF's) for the global sensitivity index (GSI), normalized by the maximum GSI value across the entire cortex. The single relatively narrow peak of the PDF for referential EEG is consistent with its relatively homogenous sensitivity across the cortical surface, as shown in figure 6. (B) Means and standard deviations of the GSI across sources and subjects for selected cortical regions. EEG measures tend to be consistent for different gyri whereas MEG measures tend to be larger for superficial than for deep areas. Abbreviations: PrG = pre-central gyrus; PoG = post-central gyrus; IFG = inferior frontal gyrus, *pars triangularis*; MTG = middle temporal gyrus; FuG = fusiform gyrus; PHG = para-hippocampal gyrus; CgG = cingulate gyrus.

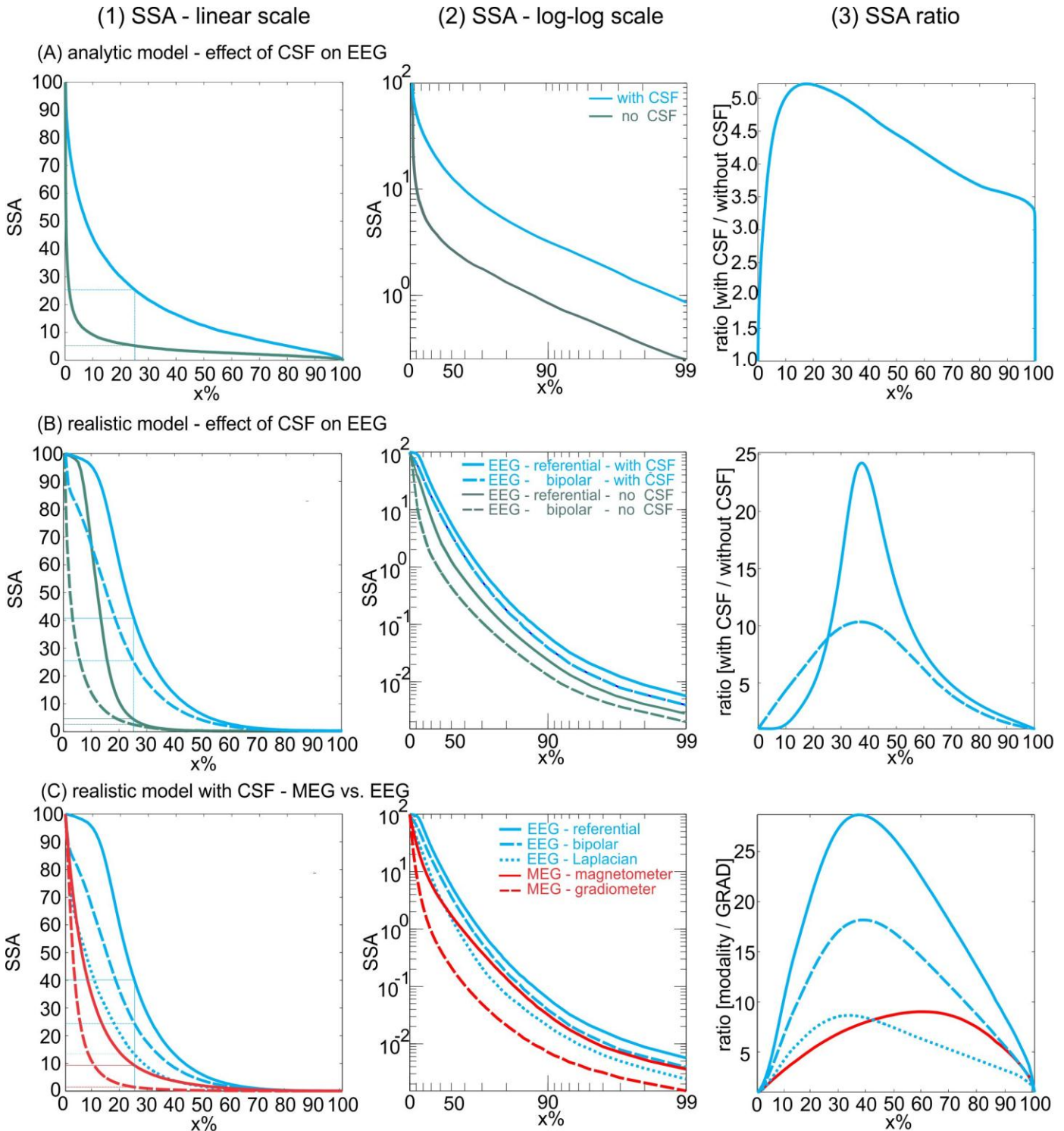
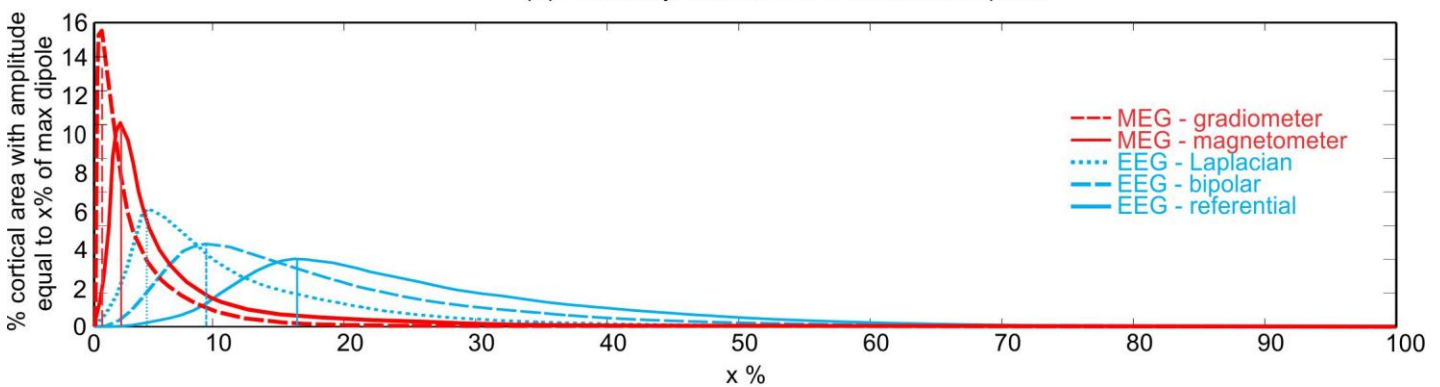


Figure 8. *Sensor Sensitivity Area (SSA)* measures for different models and modalities. SSA is the percentage of cortical dipoles that project to a given sensor at least as strongly as $x\%$ of the dipole projecting most strongly to that sensor. The curves are averages over all sensors and subjects (see text for details). (A1) Effect of CSF upon the cortical lead field of referential EEG calculated with a spherical analytic model. Including CSF raises the SSA at each $x\%$ indicating that a larger proportion of the cortical surface has that level of projection. (A2) The same data as in panel A1, plotted on a log-log scale to allow the smaller SSA at low x values to be better appreciated. Note that x has been subtracted from 100 prior to taking the log in order to accentuate the lower x values. The decreased focality when CSF is included in the model is now apparent for all values of x . (A3) Ratios of the ‘with CSF’ divided by the ‘no CSF’ SSA curves shown in panel A1. Adding CSF to the model increases the cortical area that projects with a given strength to the average sensor by a factor of 3.5 to 5. (B1) As in panel A, but using the realistic BEM model for forward calculations and the reconstructed cortical surface

for dipoles. SSA curves are shown for both referential and bipolar EEG, with or without including a sub-cranial CSF layer in the model. (B2) A log-log plot of the data in B1 shows that the effects of including CSF are maintained for all values of x . (B3) Ratios of the ‘with CSF’ divided by the ‘no CSF’ SSA curves shown in panel B1. At $x = 25\%$, adding CSF to the realistic model also increases by about eightfold the cortical area that projects with a given strength to the average sensor, regardless of whether the EEG is recorded in referential or bipolar derivations. (C1) SSA curves for different modalities and derivations. Only results based on CSF-inclusive models are displayed for EEG. Gradiometers have the lowest SSA values, indicating the greatest focality. Magnetometers are substantially less focal, comparable to Laplacian derived EEG. Bipolar EEG is clearly less focal than either MEG measure or Laplacian EEG, and referential EEG is least focal. The vertical line at $x = 25\%$ intersects the gradiometer MEG line at 1.5% (horizontal red line), indicating that for the average sensor, 1.5% of the cortical surface projects to the sensor with a strength that is $\geq 25\%$ of the strength of the strongest cortical dipole location. The same vertical line intersects the EEG referential line at 40% (horizontal blue line), indicating that over a third of the cortical surface projects to the average EEG sensor with this strength. (C2) The greater focality of gradiometers over other magnetometers and EEG extends across all values of x . (C3) Ratios of the SSA curves to different modalities and derivations, each compared to that of gradiometers (gradiometer values in the denominator of each ratio). The cortical area projecting with a given minimal strength x is up to 8 to 30 fold larger for all modalities and derivations compared to gradiometers.

(A) Probability Distribution of Lead Field Amplitude



(B) Probability Distribution of Focality

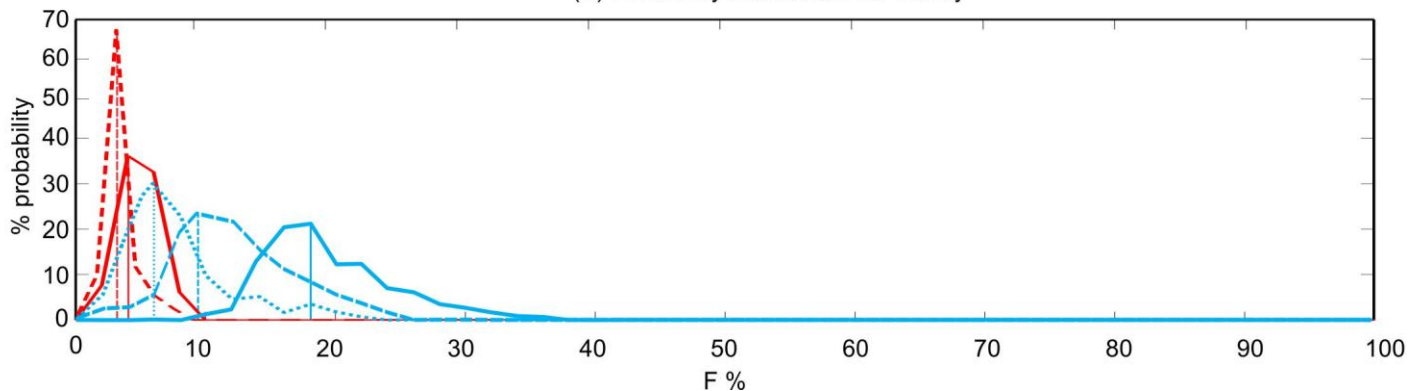
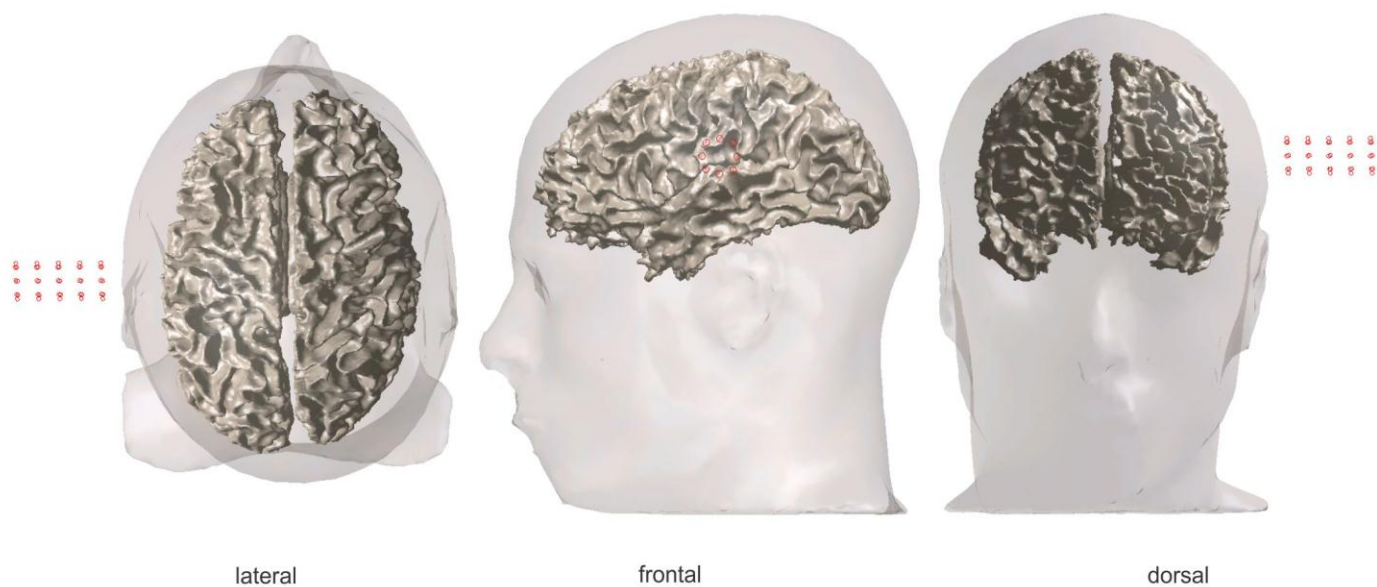


Figure 9. (A). Probability Distribution Functions (PDF's) of lead field magnitudes for each modality and derivation, averaged over all sources, sensors and subjects. The projections of every dipole to a given sensor were first normalized by the magnitude of the dipole that projected most strongly to that sensor, yielding the ‘normalized projection strength.’ The peak of the curves (equivalent to the modal value) ranges from $\sim 0.8\%$ for gradiometers to $\sim 16\%$ for referential EEG. These are the most frequent normalized projection strength from cortical sources to the respective signals. By this criterion, magnetometers are less focal than gradiometers but more focal than any EEG measure. Laplacian derivations are more focal than bipolar, which are more focal than referential. (B) Empirical PDF's of the F measure for EEG and MEG, computed over all sensors and subjects. F is the average value of the contributions across all sources to a given sensor, normalized by the largest contribution by any source. If all activity in a sensor comes from a single dipole, then F would be close to zero (1 divided by the number of dipoles in the modeled cortex, $\sim 300,000$). If all dipoles contribute equally to a given sensor, then their normalized projection strengths would all be 1, and the average of those strengths, F , would also be 1. Smaller values of F therefore indicate greater focality.

(A)



(1) SSA - linear scale

(2) SSA - log-log scale

(3) SSA ratio

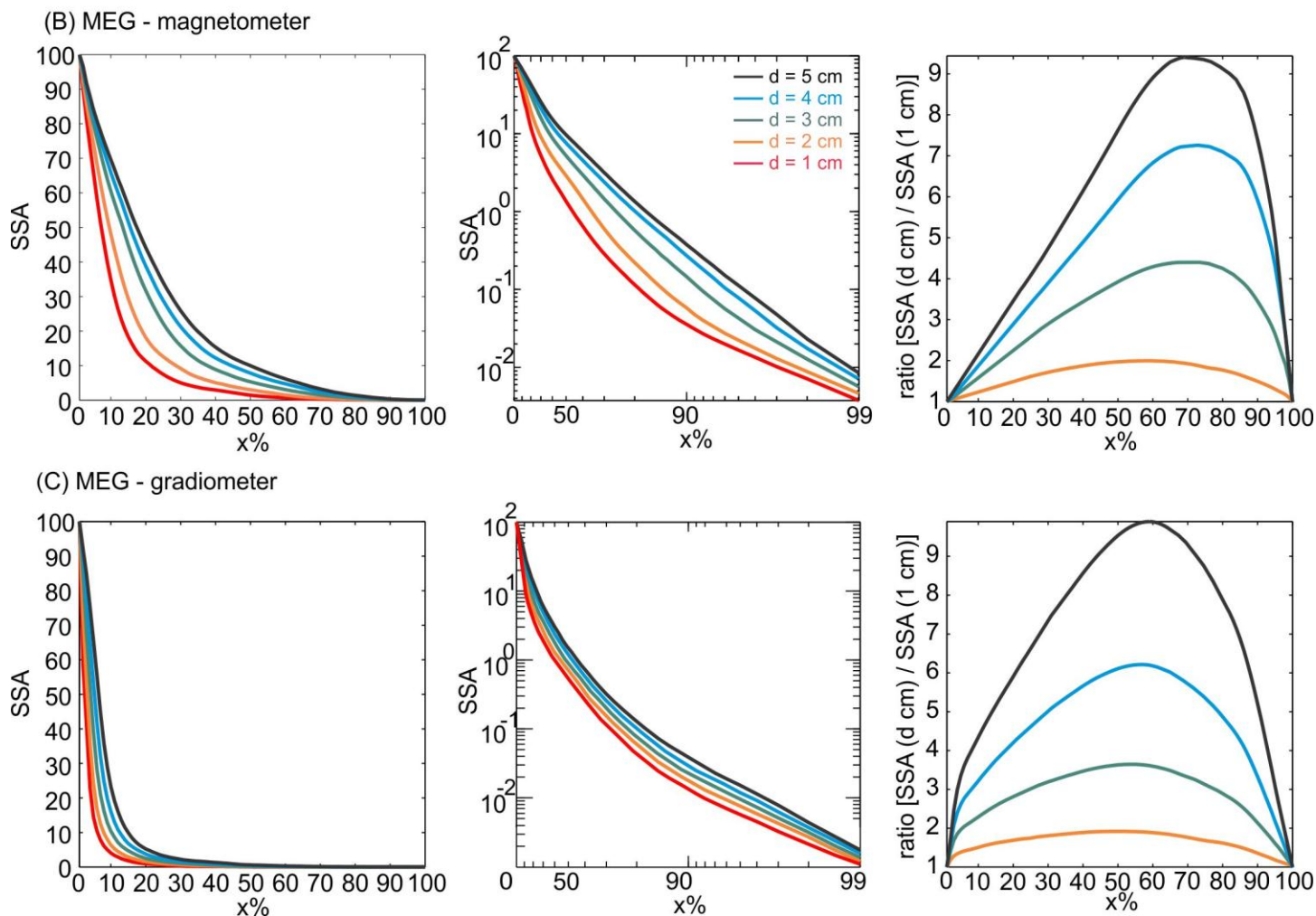


Figure 10. (A) Sample sensor locations used to explore the dependence of the *Sensor Sensitivity Area* (SSA) for MEG as a function of distance between sensor and scalp. (B) SSA as a function of distance d from MEG sensor to scalp. The curves are over one sensor and one subject (see text for details). Each color denotes a value of d as indicated. (B) and (C) display results for magnetometer and gradiometer, respectively. Panels

(B1, C1) illustrate how increasing d shifts the SSA curve upward, indicating that the modality in question is rendered less focal. Shown in (B2, C2) are the same data as in panel B1, plotted on a log-log scale to allow the smaller SSA at high x values to be better appreciated. As in Figure 8, x has been subtracted from 100 prior to taking the log in order to accentuate the lower x values. (B3, C3) Ratios of the SSA as a function of d , where d ranges from 2 to 5 cm, divided by the SSA for $d = 1$ cm. When $d = 5$ cm, the SSA when $x = 50\%$ can be over seven times larger than is the case when $d = 1$ cm.